5-17-2002

Thermochronological evolution of calcite formation at the potential Yucca Mountain repository site, Nevada: Part 2 fluid inclusion analyses and UPb dating

Jean S. Cline
University of Nevada, Las Vegas

Amy J. Smiecinski
University of Nevada, Las Vegas, smiecins@unlv.nevada.edu

Robert Bodnar
Virginia Tech

Document No.: TR-02-005.2

Document Title: Thermochronological Evolution of Calcite Formation at the Potential Yucca Mountain Repository Site, Nevada: Part 2, Fluid Inclusion Analyses and U-Pb Dating

Document Revision: 0

Originators: Nicholas S. F. Wilson and Jean S. Cline; Department of Geoscience, University of Nevada Las Vegas, 4505 Maryland Parkway, Box 454010, Las Vegas, Nevada, USA 89154-4010; and Yuri Amelin, Royal Ontario Museum, Ontario, Canada

PI (Jean S. Cline) signature: [redacted]

Date: 5/20/02

QA Manager (Amy Smiecinski) signature: [redacted]

Date: 5/20/02

Technical Reviewer: Robert Bodnar, Virginia Tech, Blacksburg, Virginia

Technical Reviewer signature: [redacted]

Date: 05/17/02

Table of Contents

Table of Abbreviations

BZ barren zone
CAZ calcite alteration zone
CL cathodoluminescence
DOE Department of Energy
DPTS doubly polished thin sections
ECRB Enhanced Characterization of the Repository Block Cross Drift
EPMA electron probe microanalyses
ESF Exploratory Studies Facility
FIAs fluid inclusion assemblages
IFZ intensely fractured zone
LA-ICP-MS ablation inductively coupled plasma mass spectrometry
LC lithophysal cavities
LCZ lithophysal cavity zone
MGSC magnesium-enriched growth-zoned sparry calcite
NP north portal
NPR north portal and ramp
NR north ramp
PMC patchy Mg-enriched calcite
PTn Paintbrush Tuff nonwelded
ROM Royal Ontario Museum
SMOW standard mean ocean water
SPR south portal and ramp
SZ saturated zone
UCCSN University and Community College System of Southern Nevada
USGS United States Geological Survey
UZ unsaturated zone
WDS wavelength dispersive spectrometry

Abstract

The presence of two-phase fluid inclusions in thin secondary mineral crusts at the potential Yucca Mountain nuclear waste repository has raised questions regarding the origin, timing, and temperature of past fluid flow through the repository horizon. The geologically recent passage of fluids with high temperatures would call into question the suitability of the site for the storage of high level nuclear waste. This study determined the thermal history of fluid flow through the site using fluid inclusion analyses and constrained the timing of thermal fluids by dating silica minerals spatially associated with the fluid inclusions using U-Pb techniques. Results provide a detailed time-temperature history of fluid migration through primary and secondary pore spaces during the past 8 to 9 million years.

One hundred and fifty-five samples were collected in the unsaturated zone from the C-shaped Exploratory Studies Facility (ESF), the ECRB cross drift which crosses the potential repository horizon, and exploratory alcoves. Detailed petrographic and paragenetic studies indicated that the oldest secondary minerals consisted of heterogeneously distributed calcite with lesser chalcedony, quartz, opal, and fluorite. The oldest secondary minerals were overgrown by intermediate bladed calcite. The youngest secondary minerals include chemically distinct Mg-enriched, growth-zoned sparry calcite (MGSC) and intergrown U-enriched opal.

Fluid inclusion petrography indicated that 50 % of the samples (n = 78) contained fluid inclusion assemblages with two-phase fluid inclusions, and that assemblages of liquid-only fluid inclusions represent > 96% of all fluid inclusions within the secondary minerals. Assemblages of two-phase inclusions also contain liquid-only inclusions that did not nucleate a vapor-bubble owing to formation at relatively low temperatures. Virtually all two–phase fluid inclusions occur in paragenetically old calcite; rare two-phase inclusion assemblages were observed in old fluorite (n = 3) and quartz (n = 2). Rare two-phase fluid inclusions were observed in early-intermediate calcite; sparse, irregularly shaped liquid-only inclusions form the only fluid inclusion assemblages observed in late–intermediate minerals and young MGSC. Homogenization temperatures for calcite across the site are generally 45 – 60 °C, but higher temperatures reaching 83 °C were recorded in the north portal and ramp of the ESF and cooler temperatures of ~ 35 – 45 °C were recorded in the intensely fracture zone. Samples from lithophysal cavities in the ESF and ECRB contain multiple populations of two-phase inclusions. Inclusion temperatures are highest in early calcite (> 45 °C) and cooler in paragenetically younger early calcite, indicating cooling with time. The cooler temperatures coincide with temperatures recorded in the intensely fractured zone and indicate that secondary minerals in the intensely fractured zone began to precipitate later than secondary minerals in other locations. Freezing point depressions determined for inclusions range from -0.2 to -1.6 °C indicating trapping of a low salinity fluid. A small number of fluid inclusions in fluorite and quartz were identified and evaluated. Four inclusions in these minerals homogenized at temperatures higher than those recorded for calcite (91 ° - 95 °C) .

Two approaches were used to constrain the timing of thermal fluids at Yucca Mountain. First, the age of MGSC was determined, and it provides a minimum age for fluids with elevated temperatures owing to the presence of only liquid-only inclusions in MGSC. Results indicate that MGSC began to precipitate across the site between 2.90 ± 0.06 Ma and about 1.95 ± 0.06 Ma, and MGSC has continued to precipitate to within the last half million years. These ages constrain fluids with elevated temperatures to have accessed the site more than about 2.90 Ma. Second, more precise temporal constraints were determined for samples in which datable opal or

chalcedony occur in the intermediate or older parts of the mineral crusts, or are spatially related to 2-phase fluid inclusions. Such ages indicate that two-phase fluid inclusions are older than 5.32 ± 0.02 Ma, and that fluids with elevated temperatures were present at Yucca Mountain before this time.

Results from this study are consistent with a model of descending meteoric water that infiltrated the cooling tuff sequence, became heated, and precipitated secondary minerals within the vadose zone. Fluid inclusions indicate that fluids with elevated temperatures were present during the early history of Yucca Mountain. Sparse, liquid-only fluid inclusions in late-intermediate to young calcite indicate that secondary minerals were precipitated from low temperature fluids during the past 5 million years. This study demonstrates that the hypothesis of geologically recent upwelling hydrothermal fluids is untenable and should not disqualify Yucca Mountain as a potential nuclear waste storage site.

1. INTRODUCTION

Yucca Mountain is unique among potential nuclear waste repository sites owing to its location underground, in the unsaturated zone (UZ), above a deep water table (Winograd, 1981). Nevertheless, the potential for dispersion of radionuclides by fluid flow through the UZ is of great concern, and site characterization has focused on constraining this flow, in part, by determining the origin of open space, secondary minerals that occur within the host Miocene tuffs. Secondary mineral crusts occur in lithophysal cavities, fractures, and breccias in the host tuffs, but the majority of the primary and secondary pore spaces contains no secondary mineral record (Whelan et al., in press).

Previous fluid inclusion studies of secondary calcite documented the presence of two-phase fluid inclusions with homogenization temperatures of 35 – 85 °C (Dublyansky, 1998; Dublyansky et al., 2001). These authors concluded that hydrothermal fluids flooded the host rocks and, as a result, they questioned the suitability of Yucca Mountain as a potential high-level nuclear waste repository. However, the timing of the presence and trapping of fluids with elevated temperatures and their sources were not known.

A major goal of this study was to determine when fluids with elevated temperatures were present at Yucca Mountain. Ambient temperatures at Yucca Mountain are about 27 °C. However, we do not know what past ambient temperatures were at Yucca Mountain. Two-phase, liquid-vapor fluid inclusions form because trapped fluids cooled and contracted. Therefore, two-phase fluid inclusions clearly document the former presence of fluids with elevated temperatures. In this study we documented two-phase fluid inclusions that homogenized at temperatures of 35 °C and higher, and we consider fluid temperatures of about 35 °C and higher to be elevated.

To conduct this study, samples were collected from the Exploratory Studies Facility (ESF), Enhanced Characterization of the Repository Block Cross Drift (ECRB), and exploratory alcoves (Fig. 1), and detailed petrographic, geochemical, and isotopic studies were conducted. Initial work focused on constructing a paragenetic sequence for secondary mineral occurrences across the site (Wilson and Cline, 2002). Subsequent work, reported here, integrates the paragenetic study with fluid inclusion and geochronology studies to address four specific questions: 1) Did fluids with elevated temperatures invade the repository site? If an influx of fluids with elevated temperatures occurred, 2) how widespread within the repository site was this influx? 3) what were the temperatures of the fluids that invaded the site? and 4) when did these fluids invade the site?

2. BACKGROUND AND PREVIOUS RESEARCH

2.1. Geological Background

Yucca Mountain was originally identified as a possible high-level geologic nuclear waste repository for a number of reasons. In particular, this region has an arid climate with less than 25 cm of rain per year (U.S. DOE, 1988), and a deep unsaturated zone with a water table 400 – 600 m below the present day surface (Winograd, 1981). The mountain is located 90 miles northwest of Las Vegas at the western edge of the Nevada test site, within the Southwest Nevada Miocene volcanic field (Christiansen et al., 1977). Comprehensive discussions of the geology at Yucca

Mountain are given by Sawyer et al. (1994), Buesch et al. (1996), and Stuckless and Dudley (in press), and have been briefly summarized by Wilson and Cline (2002).

Yucca Mountain is composed of a 1 – 3 km thick sequence of shallowly eastward dipping felsic welded and non-welded volcanic tuffs of the Paintbrush Group (Sawyer et al., 1994; Wilson and Cline, 2002; their Fig. 1). The Paintbrush Group comprises the Topopah Spring, Pah Canyon, Yucca Mountain, and Tiva Canyon Tuffs (Sawyer et al., 1994). The Topopah Spring Tuff, dated at 12.8 Ma, directly overlies bedded rhyolite tuffs of the Calico Hills Formation and is overlain by the thin Pah Canyon and Yucca Mountain Tuffs (Sawyer et al. 1994), collectively know as the PTn. The Tiva Canyon Tuff, dated at 12.7 Ma, overlies the PTn (Sawyer et al., 1994). Younger faulting related to Basin and Range extension (e.g. Stewart, 1988) cuts the tuff sequence. Basaltic eruptions formed flows and cones during the late Tertiary in Crater Flat with the most recent episode creating the Lathrop Wells Cone about 75 Ka (Heizler et al., 1999).

To enhance site characterization, two tunnels were excavated into the mountain near the potential repository (Fig. 1). The ESF crosses the Topopah Spring, Pah Canyon, Yucca Mountain, and Tiva Canyon Tuffs; the ECRB was excavated entirely within the Topopah Spring tuff about 15 m above the potential repository horizon. All samples used in this study were collected from the ESF, ECRB, and exploratory alcoves in the UZ. The UZ extends from the surface to a depth of around 500 – 700 m where the water table is encountered and the saturated zone (SZ) begins. The potential repository is to be situated in the lower member of the Topopah Spring Tuff, ~ 300 m below the surface and above the water table.

Within the UZ, primary and secondary porosity occur as lithophysal cavities (LC), fractures, and breccias. LC are roughly parallel to bedding and formed as gas exsolved from the cooling tuff sequence. This gas exsolution led to early high-temperature vapor-phase alteration along the margins of LC and cooling fractures. Alteration produced bleached margins and secondary minerals that are sub-parallel to bedding (vapor-phase partings) and include predominantly tridymite, cristobalite, alkali feldspar, and hematite (Carlos, 1994; Levy et al., 1996).

The majority of primary and secondary pore spaces in tuffs at Yucca Mountain remain open and contain no secondary mineral record (Whelan et al. 1996; Whelan et al., in press; Wilson and Cline, 2002). Where present, secondary minerals are restricted predominantly to the footwalls and bases of LC, fractures, and breccias (Whelan et al. 1996; Wilson and Cline, 2002). Paragenetic studies by two groups (Whelan et al., in press; Wilson and Cline, 2002) led to similar conclusions in regards to the sequence of secondary mineral precipitation following deposition of vapor-phase minerals. Early minerals were represented by calcite with lesser chalcedony, quartz, opal, and fluorite and were heterogeneously distributed across the site. These minerals were overgrown by intermediate minerals composed primarily of distinctive calcite blades. Outer 'late stage' calcite observed by Whelan et al. (in press) was typically clear and had distinctive C and O isotopic signatures and the authors concluded that this calcite could be correlated across the site based on a combination of petrography and C and O isotopic signatures (Paces et al., 1997). Wilson and Cline (2002) observed that the outer late stage calcite represented the most recently deposited secondary mineral at Yucca Mountain. They further determined that this calcite is chemically distinct and contains fine growth zones containing up to ~ 1 wt.% Mg. Termed Mg-enriched, growth-zoned sparry calcite (MGSC), this layer can be distinguished from all other calcite by its chemistry and growth zoning, is associated and intergrown with clear opal, occurs in > 65 % of the samples studied, and can be correlated across the site.

2.2. Fluid Inclusion Studies

Previous fluid inclusion studies of secondary mineral crusts have led to conflicting interpretations. Initial studies of UZ calcite from drill core samples were published by Bish and Aronson (1993) and Roedder et al. (1994). Bish and Aronson (1993) focussed on SZ calcite which contained 2–phase inclusions that formed at temperatures up to 250 °C. Roedder et al. (1994) observed primary inclusions in calcite from drill core with variable liquid-vapor ratios and the majority of inclusions were either all liquid or all vapor. They concluded that the inclusions were trapped at near surface temperatures in the vadose zone. Roedder and Whelan (1998) presented additional data from samples from the ESF and drew similar conclusions. Dublyansky and co-authors, however, produced several reports (e.g. Dublyansky, 1998; Dublyansky et al., 1998; Dublyansky et al., 2001) in which they concluded that secondary minerals formed in a phreatic environment. They suggested that calcite precipitated from upwelling hydrothermal fluids that flooded the repository horizon on multiple occasions, including during the recent geologic past. Dublyansky (1998) showed that fluid inclusion assemblages (FIAs) in calcite contained both two–phase inclusions with consistent liquid-vapor ratios and liquid-only inclusions. Several FIAs exhibited consistent homogenization temperatures over a range of 35 – 85 °C, temperatures that are higher than the present day temperature of the water table (~ 32 °C) (Dublyansky et al., 2001). Freezing point depressions of 0 °C to -1.25 °C indicated inclusion salinities that the authors concluded were too high for vadose zone waters.

The lack of recognition of FIAs containing two-phase fluid inclusions in early studies by Roedder et al. (1994) and Roedder and Whelan (1998) may be related to handling of the samples used in these studies (Whelan et al., in press). The inclusions in the samples may have homogenized during collection, storage, or section preparation (Whelan et al., in press) and, as they do not readily renucleate a vapor bubble after homogenization, two-phase fluid inclusions would not have been available for identification. More recent work by Whelan et al. (in press) based on samples that were properly handled, recognizes the presence of FIAs with consistent liquid-vapor ratios in secondary minerals at Yucca Mountain.

The limited petrographic information presented in studies by Dublyansky and coworkers precludes placing the reported fluid inclusion data in any temporal context. The current study was initiated to confirm the presence of FIAs containing fluids with elevated temperatures and to constrain the ages of these fluid inclusions and the timing of fluid access to Yucca Mountain.

2.3. U–Pb and U–series Studies

Secondary opal and chalcedony intergrown with calcite locally contain high U and very low common Pb and ^{232}Th. These trace element concentrations make micro-samples of opal and chalcedony suitable for precise U-Pb (Neymark et al., 1998) and U-Series dating (Neymark and Paces, 1996, 2000; Paces et al., 1996, 1998a, Neymark et al., 1998, Neymark et al., 2000). Geochronological studies were previously conducted to investigate the timing of secondary mineral deposition and the depositional rate, which are, in turn related to fluxes through the UZ (Neymark et al., 1998). Opal and chalcedony were dated using U-Pb and have provided ages ranging from 0.1 – 10 Ma, indicating that secondary mineral formation initiated within 2 Ma of tuff emplacement; sequentially younger ages were obtained for outermost opals (Neymark et al., 1998). Chalcedony at the base of some mineral crusts gave the oldest ages of 8 – 10 Ma, whereas clear opals, typically in intermediate to youngest stratigraphic positions, have younger ages. The

older ages from chalcedony were interpreted to be consistent with late-stage magmatic activity in the Timber Mountain caldera (Neymark et al., 1998). Neymark et al. (1998) suggested that depositional rates of 1 – 4 mm/Ma in the potential repository horizon were consistent throughout the Neogene and Quaternary and have not varied substantially during the last 8 million years. These depositional rates are consistent with U-series data and led to a model describing continuous secondary mineral deposition at a constant, slow rate to the present (less than 5 mm/Ma; Neymark and Paces, 2000). Data derived from in-situ SHRIMP analyses of opal growth zones (Paces et al., 2000) indicate similar growth rates.

3. SAMPLING AND ANALYTICAL METHODS

3.1. Sample Collection

One hundred and fifty-five samples of secondary minerals and adjacent wall rock were collected from LC, fracture, and breccia occurrences from the ESF, ECRB, and exploration alcoves at Yucca Mountain (Fig. 1). All styles of secondary mineral occurrences identified within the site were sampled. Samples were maintained at temperatures between 0 – 35 °C during sampling, transportation, thin section preparation, and storage, according to UCCSN Quality Assurance (QA) procedures, so as not to adversely affect the fluid inclusions.

The tunnels and alcoves have been divided into six zones (Fig. 1) based on local differences in secondary minerals, mineral occurrences, and fluid inclusion homogenization temperatures. Samples from the north portal (NP) and north ramp (NR) are fracture and breccia occurrences and typically contain more silica minerals than samples from other areas of the site. Samples from the lithophysal cavity zone (LCZ) and the ECRB are primarily from LC occurrences and contain predominantly calcite with some chalcedony-quartz and clear opal. The intensely fractured zone (IFZ) contains steeply dipping fractures that contain calcite with minor early fluorite. South portal and ramp (SPR) samples are from LC, fracture, and breccia occurrences and contain variable amounts of calcite, chalcedony and opal. These zones are similar to zones presented by Wilson and Cline (2002) except that the north portal and north ramp are separated in this report, rather than being combined into a single zone.

3.2. Fluid Inclusion Petrology and Microthermometry

Doubly polished thick sections (DPTS) for fluid inclusion studies were prepared so as to limit heating and fracturing of the samples (Wilson and Cline, 2002). A critical component of this study was the selection of fluid inclusions for analysis that were identified as comprising fluid inclusion assemblages (FIAs) (Goldstein and Reynolds, 1994). An FIA is a petrographic classification that describes a group of fluid inclusions that were formed at the same time and, therefore, at the same temperature and pressure. All inclusions that are part of an FIA may not homogenize at the same temperature owing to post trapping modification of some inclusions. Fluid inclusions in an FIA may also exhibit different phase relations. Most fluid inclusions examined in this study were determined to be primary, based on their occurrences within growth zones; a small number of fluid inclusion assemblages occurred in fractures indicating they are secondary. Fluid inclusion petrography was integrated with the secondary mineral paragenesis;

genetic relationships between primary FIAs and various stages of secondary minerals were determined and provided relative ages for primary FIAs.

Homogenization and ice melting measurements were collected on a Linkam THMSG 600 heating and freezing stage attached to a CI 93 programmer and LNP cooling pump. The equipment was controlled by LinkSys software version 1.83. The Linkam stage is mounted on an Olympus BX60 microscope and a Polaroid DCM IE digital camera was used to capture images. Synthetic fluid inclusions were used to calibrate the stage at 374.1 °C, 0.0 °C, and -56.6 °C and stage calibration was checked each day prior to analysis. Chips from the DPTS were left attached to glass slides during microthermometry, because the samples tended to break apart if removed from the slide.

Homogenization temperatures for selected inclusions in an FIA in each chip were determined during a single heating run beginning at 35 °C. During each run temperatures were cycled by increasing the temperature 2 °C above the temperature of the previous cycle, and then cooling the sample a few degrees. Homogenization was assumed for each inclusion in which the vapor bubble was no longer present after heating. Freezing studies were conducted after heating studies to avoid freeze-stretching of the fluid inclusions (Lawler and Crawford, 1983). Since the two-phase fluid inclusions did not renucleate a vapor bubble on cooling following inclusion homogenization, the chips were heated to ~ 150 °C to stretch the inclusions for ice melting determinations. Stretching increased the possibility of generating vapor bubbles in the inclusions for freezing studies to estimate fluid inclusion salinities. Ice melting temperatures were determined by monitoring the expansion and contraction of the vapor bubble as temperatures were cycled at sub-zero temperatures. In the majority of samples examined, vapor bubbles did not nucleate and salinities could not be determined because ice-melting temperatures in the absence of a vapor bubble cannot be used to determine salinity (Roedder, 1984).

3.3. δD Composition of Inclusion Fluids

Hydrogen isotope signatures were determined for selected fluid inclusion assemblages following the method of Sharp et al. (2001). Sample material was removed from billets from which the examined polished sections were prepared, from equivalent slices of secondary mineral crusts. Only samples that contained consistent single fluid inclusion populations were analyzed. Examination of as many as five polished sections from a single sample showed that samples were consistent from section to section, indicating that material examined in section could be collected from the billet for analysis. Calcite samples were thermally decrepitated using a CO_2 laser and evolved H_2O from the fluid inclusions was reduced to H_2 by glassy carbon at 1450 °C in a He carrier gas. H_2 was separated in a gas chromatograph and analyzed by a Finnigan MAT Delta^{Plus} XL mass spectrometer. The instrument and analytical setup were calibrated using NBS and other secondary standards for H. Results have a precision of ± 2 ‰ and are reported relative to Vienna SMOW.

3.4. U-Pb and U-series Dating

Opal and chalcedony used for dating were hand picked under a binocular microscope from pieces of DPTS that were soaked in acetone to allow easy separation of opal from calcite. Darker opal and chalcedony were generally collected from layers and irregular growths in paragenetically older parts of mineral crusts. Clear opal samples are generally present in and

were collected from thin continuous or discontinuous layers within paragenetically younger layers of the mineral crusts.

U–Pb and ^{230}Th–U analyses were carried out using the technique described by Neymark et al. (2000) at the Jack Satterly Geochronology Laboratory, Royal Ontario Museum (ROM), Toronto, Canada. The samples were spiked with the mixed ^{205}Pb–^{229}Th–^{233}U–^{236}U tracer solution prior to dissolution, and U–Pb and U–series isotopic data were obtained from the same aliquot. Isotopic compositions of U, Th and Pb were measured using thermal ionization mass-spectrometer VG–354, recently equipped with ion counting Daly photomultiplier detectors. Ion counting provides improved precision in the analyses of small and low–U samples compared to the previously used analog Daly detectors (Neymark et al. 2000).

Isotopic analyses were corrected for procedure blanks measured with each batch of samples. Concentrations of Pb, U, and Th in procedure blanks used in the sample data reduction were taken from the blank measurements performed together with the same batch of samples or from the immediate preceding batch. In those cases where more than one blank measurement was taken with the same batch of samples, the blank values were averaged for sample data reduction. The total procedural blanks measured during this study varied between 0.3 – 0.9 pg Pb and 0.3 – 2.0 pg U and Th. The representative blank Pb isotopic composition values were obtained as weighted averages of the ROM Geochronology Lab blank database over the period of 1996 to 2000 as 18.76 ± 0.21 (^{206}Pb/^{204}Pb), 15.58 ± 0.094 (^{207}Pb/^{204}Pb), and 38.02 ± 0.27 (^{208}Pb/^{204}Pb). The blank Pb isotopic compositions measured together with the silica samples are consistent with the database average values.

The precision and accuracy of the ^{234}U/^{238}U and ^{230}Th/^{238}U activity ratio measurements were additionally checked using a solution of a secular equilibrium material (~70 Ma old uranium ore, Ludwig et al., 1985). The results of repeated analyses (Fig. 2) are reproducible within the 2σ error limits, and weighted means of the ^{234}U/^{238}U and ^{230}Th/^{238}U activity ratios are within analytical error of unity. The Pb isotopic compositions used in the initial common Pb corrections, and the decay constant values are the same as reported previously.

4. FLUID INCLUSION ANALYSES

4.1. Fluid Inclusion Petrography

Three types of fluid inclusions are present at Yucca Mountain. 1) Liquid-only inclusions are the most abundant fluid inclusions in secondary minerals and they constitute more than 96 % of all inclusions observed. 2) Two–phase, liquid-plus-vapor inclusions are sparse (< 3 %) and 3) vapor-only inclusions are rare (< 1 % of inclusions). A small number of assemblages (< 1 %) of liquid plus vapor inclusions contain inclusions with variable liquid-vapor ratios. Most two-phase inclusions have small vapor bubbles, exhibit consistent liquid-vapor ratios, and coexist in FIAs with liquid-only inclusions. The two-phase and liquid-only inclusions in these assemblages were trapped at the same time under the same conditions, constituting a valid FIA; however, because of the relatively low trapping temperatures, some of the inclusions did not nucleate a vapor bubble on cooling. Most of these inclusion populations are in calcite (>99 %), but a small number of FIAs containing liquid plus vapor inclusions were identified in quartz and fluorite. These low-temperature FIAs that contain the liquid plus vapor and liquid-only inclusions are referred to as 2-phase FIAs in this report, distinguishing them from assemblages of liquid-only

inclusions. Although these 2-phase FIAs are not abundant, they are relatively common in some mineral layers in some samples.

FIAs of liquid-only inclusions, the most abundant inclusions at Yucca Mountain, occur in early to early-intermediate calcite (Fig. 3) in some samples. These inclusions are typically primary, and inclusions are aligned along growth zones (Fig. 4a). Liquid-only inclusions comprise the only inclusion assemblages in bladed calcite and MGSC, and the abundance of inclusions is significantly decreased in this calcite. The liquid-only inclusions are irregularly shaped and are elongated along growth zones (Fig. 4b). Outermost MGSC is commonly clear and generally contains no inclusions, but locally exhibits dark micropores between growth zones. Some of these pores contain rare, primary liquid-only inclusions.

Sparse 2–phase FIAs are most abundant in calcite, are generally primary, and are usually aligned along growth zones in three-dimensional arrays in the cores of crystals or in calcite blades (Fig. 4c). Primary inclusions illustrated in Figure 4c are typical of 2–phase FIAs found in calcite and evaluated using microthermometry. A few 2–phase FIAs lie along fracture planes and are secondary or are of unknown origin. Typically, the homogenization temperatures of the 2-phase FIAs are consistent and temperatures are always less than 100 °C. Some inclusions with inconsistent liquid-vapor ratios (vapor-bubbles ~10 – 80 volume %) and large vapor bubbles (Fig. 4d) occur within an FIA in which the large majority of the inclusions show consistent liquid-vapor ratios and consistent homogenization temperatures. These textural relationships suggest that the inclusions with large bubbles and inconsistent liquid-vapor ratios have leaked.

Figure 3 summarizes the paragenetic sequences of secondary minerals observed by Wilson and Cline (2002) at Yucca Mountain and incorporates the distribution of fluid inclusion populations. Two–phase FIAs occur in paragenetically early calcite around and adjacent to the wall rock at the base of secondary crusts, often within a few millimeters of the wall rock. A small number of 2–phase FIAs were identified in the basal parts of bladed calcite, generally where blades are small and growth zones are broad (Fig. 3). Vapor bubbles are slightly larger in 2–phase FIAs in basal calcite and are smaller in paragenetically younger calcite. The paragenetically youngest 2–phase FIAs observed were identified in a single sample in calcite that precipitated with early-intermediate opal. Two-phase FIAs do not occur in the central and outermost parts of calcite blades, or in the larger and more slender intermediate-stage calcite blades. In these calcites rare liquid-only inclusions were identified (Fig. 3). In addition, no 2–phase FIAs are present in paragenetically youngest MGSC.

Rare 2–phase FIAs occur in paragenetically early to earliest intermediate quartz ($n = 2$) and fluorite ($n = 3$) (Wilson and Cline, 2002). These FIAs are in the basal parts of crusts adjacent to and around the wall rock, and are overgrown by later secondary minerals (Fig. 3). Quartz is usually clear and inclusion free but locally exhibits darker patches of small liquid-only inclusions (< 10 μm diameter). Rare quartz contains primary 2–phase FIAs and inclusions have liquid-vapor ratios that are similar to 2–phase FIAs in adjacent calcite (vapor bubbles < 1 % volume). Two generations of fluorite have been identified. Earliest fluorite forms nodules and masses that are generally about 0.5 mm, but which may reach one or more millimeters, and which may contain 2–phase FIAs. Some of the 2-phase FIAs are primary and occur in the cores of crystals; others are of unknown origin. Small fluorite cubes, in which 2–phase FIAs have not been observed, are present in early to intermediate secondary minerals (Wilson and Cline, 2002).

Vapor-only inclusions are locally present at the base of some of the mineral crusts (Fig. 3). Some of these inclusions are large and "faceted," exhibiting near-negative crystal shapes. Two-phase inclusions with variable liquid-vapor ratios and dark vapor bubbles are present in a

number of samples. These inclusions are commonly spatially associated with 2–phase FIAs at the base of crusts (Fig. 4d). The two-phase inclusions with the dark vapor bubbles occur dominantly at the base of lithophysal cavity crusts and have been observed in calcite, but not in other minerals. During heating the liquid-vapor ratios and dark vapor-bubbles did not noticeably change. It is unclear whether these inclusions formed by heterogeneous trapping or by leaking after trapping. Owing to the ambiguous origin of these inclusions and their restriction to the oldest parts of the mineral crusts in a small number of samples, they are not discussed further.

4.2. Spatial Distribution of 2-Phase FIAs

Two-phase FIAs have been observed in 78 of 155 samples (~ 50 %). The FIAs are present in secondary minerals from sample locations across the site (Fig. 1) and occurrences are split almost evenly between LC (~ 51 %) and fractures / breccias (~ 49 %). Two-phase FIAs are most common in the LCZ and the eastern part of the ECRB, and are rarer in the NP and SPR. Approximately half of the samples in the IFZ contain 2–phase FIAs. The distribution of 2-phase FIAs indicates that fluids with elevated temperatures accessed pore spaces that contain secondary minerals across the site. However, the distribution is erratic and samples that contain 2–phase FIAs are commonly adjacent to sample sites that lack 2–phase FIAs.

4.3. Fluid Inclusion Microthermometry

Sixty-one of the 78 samples that contain 2–phase FIAs were examined using microthermometry and more than 2500 inclusions were heated to determine homogenization temperatures. The temperatures determined for 2–phase FIAs in calcite across the site have a range of 35 – 83 °C (Fig. 5). Two-phase FIAs from all occurrences (LC, fractures, and breccias) in the LCZ, SPR, and ECRB provided homogenization temperatures of 35 – 67 °C. Inclusions in calcite from the NP and NR have homogenization temperatures that reach 83 °C and 75 °C, respectively, whereas most inclusions in the IFZ homogenize below 50 °C. Stratigraphic reconstructions at Yucca Mountain indicate that there has been minimal erosion since the volcanic rocks were deposited (S. Levy, personal communication, 1999) and it is generally accepted that no more than 100 m of overlying rocks have been eroded from the surface of Yucca Mountain. Such a low erosion rate indicates that the inclusions were trapped at depths of less than 400 m and, as a result, homogenization temperatures approximate inclusion trapping temperatures and do not require a pressure correction. Note that if the inclusions were trapped in a vadose environment the homogenization temperatures equal the trapping temperatures and no pressure correction is needed (Roedder and Bodnar, 1980).

Primary 2–phase fluid inclusions in individual FIAs (Fig. 4c) provided consistent homogenization temperatures. In many samples, multiple FIAs produced nearly identical data. Inclusions in most FIAs homogenized within a range of about 10 °C and in many FIAs, all inclusions homogenized over a range of about 6 °C. Figure 6 illustrates the consistency of homogenization temperatures for 181 fluid inclusions in sample ESF 01+62.3 from the NP. Most inclusions homogenized from 61 – 67 °C, a temperature range of 6 °C. Data include all homogenization temperatures from one chip and data from six FIAs identified in a second chip. These results show that a single FIA is representative of all data from this sample.

During microthermometry a few inclusions in measured FIAs homogenized at somewhat scattered, higher temperatures than the bulk of the data. Such temperatures probably reflect

stretching of calcite during heating. These data are not shown in Figure 5 and their removal does not change the mode or the range of the majority of the data. The consistency of homogenization temperatures for inclusions of different sizes reinforces the conclusion that the evaluated inclusions are part of an FIA (Goldstein and Reynolds, 1994), that the 2–phase FIAs trapped a single homogeneous fluid, and that the inclusions were not heated or perturbed by subsequent events.

Two-phase FIAs in calcite from lithophysal cavities in the Topopah Spring Tuff in the LCZ and ECRB exhibit bimodal distributions of homogenization temperatures. Samples from the LCZ have modes at 47 – 57 °C and 39 – 41 °C; samples from the ECRB have modes at 49 – 57 °C and 43 – 47 °C (Fig. 5). Higher temperature fluids were trapped in older calcite whereas lower temperature fluids were trapped by paragenetically younger calcite indicating a cooling trend with time. The low temperature modes are similar to homogenization temperatures of inclusions in fracture and breccia occurrences in the IFZ (Fig. 5), which have a mode of 41 – 49 °C. The low homogenization temperatures in samples from the IFZ suggest that fracture- and breccia-related calcite probably had not precipitated when the earliest, higher temperature fluids invaded the site. The lack of vapor phase minerals in these samples is consistent with their later formation. These observations suggest that the various temperature ranges recorded across the site reflect fluid fluxes that occurred at different times, and are consistent with a temperature decline over time.

Inclusions in calcite samples from lithophysal cavities, fractures, and breccias from the SPR exhibit a single mode of homogenization temperatures at about 53 – 59 °C. This mode is slightly higher than modes determined for the LCZ and ECRB (Fig. 5).

The highest homogenization temperatures in calcite were recorded in samples from the NP and NR. Inclusions in two samples from the Tiva Canyon Formation in the NP (Figs. 1 and 5) have homogenization modes of about 73 – 79 °C and 61 – 67 °C. In both samples 2–phase FIAs are paragenetically early and are overgrown by younger calcite that contains rare, liquid-only FIAs. Many samples from the NP contain calcite; however, very few samples from this locality contain 2–phase FIAs. This distribution highlights the localized presence of 2-phase FIAs and especially, the localization of these highest homogenization temperatures. Inclusions in samples from the NR (Fig. 5) exhibit a large mode of homogenization temperatures from about 51 – 65 °C with temperatures extending to 75 °C. Secondary mineral distribution in this zone is quite variable with some samples containing more silica than calcite. Secondary mineral crusts also have variable thicknesses, and cemented breccias are locally present. Inclusion homogenization temperatures were consistent across the breccia samples indicating that there was little variation in temperature as the cementing calcite was deposited. The data for the NR indicate that, where 2-phase FIAs are present, the calcite in these samples precipitated at temperatures slightly greater than temperatures recorded over most of the Yucca Mountain site (Fig. 5).

In samples that contain multiple 2-phase FIAs that provide different ranges of homogenization temperatures, temperatures consistently decline with age of the inclusions and host minerals. Relatively simple crusts, in which calcite precipitated layer by layer from the base of the section outward, most clearly show this relationship. Basal calcite in sample ESF 27+84 from a lithophysal cavity (Fig. 7a) contains 2-phase inclusions at the base that homogenized from 48 – 53 °C. In younger calcite, inclusion homogenization temperatures become lower and temperatures from 37 – 43 °C were recorded in the outmost layer that contains 2-phase FIAs. Younger calcite in this sample contains only liquid-only inclusions. Sample Al#5 00+28.5 (Fig.

7b) exhibits a similar trend of decreasing temperature in paragenetically younger calcite. It is somewhat more difficult to identify the precipitation sequence of secondary minerals in fracture and breccia samples especially in samples in which multiple tuff clasts are cemented and rimmed by calcite. Nevertheless, even these samples (Figs. 7c and 7d) show a decline in temperature from identifiable older basal layers to younger layers; MGSC containing only liquid-only inclusions forms the youngest layers.

Two-phase FIAs were only observed in two samples of quartz and three samples of fluorite and the limited data are presented in Figure 8. The small number of homogenization temperatures is generally consistent with data obtained from calcite. The highest homogenization temperatures were obtained from inclusions in a sample from the NP. Inclusions in quartz from this sample have homogenization temperatures that range from 73 – 95 °C and are less consistent than temperatures typically obtained from calcite. Two-phase inclusions in paragenetically early fluorite from the same sample leaked during heating. Both quartz and fluorite in this sample (ESF 05+57.1) are present at the base of the mineral crusts, are overgrown by chalcedony, and are paragenetically old. Although the temperature range for quartz is rather large for an FIA (e.g. Goldstein and Reynolds, 1994) the data indicate that quartz and probably fluorite in the NP formed at temperatures similar to and slightly higher than temperatures obtained for calcite in this locality. Inclusions in quartz and fluorite from other localities provided lower homogenization temperatures, similar to calcite. Sample ESF 22+19 contains primary 2–phase inclusions in quartz that homogenized from 53 – 71 °C (Fig. 8). Inclusions in calcite adjacent to the quartz homogenized at 53 – 57 °C (n = 10). Sample ESF 53+35.5 contains paragenetically early fluorite that precipitated on wall rock. This fluorite contains 2–phase FIAs that have homogenization temperatures of 43 – 53 °C, identical to homogenization temperatures obtained in adjacent calcite. In sample ECRB 25+30 fluorite that precipitated on wall rock contains 2–phase FIAs, all but two of which homogenized at 69 – 81 °C (n = 21; 2 assemblages). Calcite surrounding this fluorite contained only liquid-only inclusions indicating formation at lower temperatures.

The integrated secondary mineral paragenesis, fluid inclusion petrography, and heating studies demonstrate the presence of a single, consistent cooling trend with time. Two-phase FIAs with the highest homogenization temperatures occur in secondary minerals growing around the wall rock or in minerals spatially associated with wall rock at the base of mineral crusts. The high temperatures recorded in NP and NR samples are in paragenetically old material and may record the earliest fluid fluxes through the Yucca Mountain site. Two-phase FIAs with lower homogenization temperatures occur in early-intermediate secondary minerals, and are the only inclusions trapped in secondary minerals associated with fractures and breccias in the IFZ. In samples that contain modes of both higher and lower homogenization temperatures, the higher temperature inclusions are always present in paragenetically older minerals. Intermediate bladed calcite and youngest MGSC only contain liquid-only inclusions, demonstrating continuation of the cooling trend to youngest calcite. As most of the evaluated inclusions are primary, these homogenization temperatures reflect declining temperature conditions across the site as the secondary minerals precipitated.

Homogenization temperatures are clearly not related to a paleogeothermal gradient and are, in fact, inversely related to depth. Samples containing the fluid inclusions with the highest observed homogenization temperatures are from the NP, which is at a current depth of 0 – 55 m. The LCZ and ECRB are located at depths below the surface of greater than 185 m and inclusions in both areas trapped fluids with intermediate to low temperatures. Samples from the IFZ that

trapped only the coolest fluids are from the deepest part of the ESF (215 – 270 m). These temperatures, furthermore, are not related to a lateral temperature gradient across the site because the temperature variations occurred at different times. The distribution of fluid inclusion homogenization temperatures is related to precipitation of secondary minerals from fluids that declined in temperature over time.

4.4. Fluid Inclusion Ice Melting Temperatures

Ice melting temperatures were obtained for 129 inclusions from 2-phase FIAs in calcite from 30 samples across the site (Fig. 9). The data are limited owing to the difficulty in nucleating vapor bubbles necessary for the analyses. Temperatures range between -0.2 and -1.6 °C, and the majority of the temperatures are between -0.4 and -0.9 °C. These temperatures indicate a salinity range of 0.35 to 2.74 wt.% NaCl equivalent (Bodnar, 1993), with the majority of the data ranging from 0.71 to 1.57 wt.% NaCl equivalent. Given that the inclusions are trapped in calcite, trace CO_2 in the fluid is contributing to the freezing point depression.

There is no systematic relationship between homogenization and ice melting temperatures. For example, ice melting temperatures for inclusions in fluorite (ECRB 25+30) are between -0.6 °C and -0.7 °C and homogenization temperatures range from 69 – 81 °C. These ice melting determinations are the same as the majority of the data for calcite, including samples from the IFZ that formed at < 50 °C. Results indicate that the 2–phase FIAs consistently trapped a low-salinity fluid.

4.5. δD Compositions of Fluid Inclusion Fluids

Three calcite samples were analyzed to determine the δD composition of the fluids trapped by various inclusion populations (Table 1). Samples were collected from intermediate calcite that contained 2–phase FIAs and was well constrained by U-Pb dating, and from MGSC that contained rare all liquid inclusions. δD compositions varied between -90 ‰ and -131 ‰. Intermediate calcite (AL#5 00+28.5) had a composition of -90 ‰ to -120 ‰, and the youngest MGSC (ESF 27+84, ESF 60+52.5) had isotopic signatures of -110 ‰ to -131 ‰. These data indicate that the inclusions trapped meteoric fluids.

5. U–Pb DATING

Opal and chalcedony in the secondary mineral layers were dated using U-Pb and U-series methods to constrain the ages of the 2–phase FIAs. Based on the distribution and availability of datable minerals in the sections, the strategy of the geochronology study was to 1) determine the age of MGSC, which provides a minimum age for the 2–phase FIAs, and 2) place more precise constraints on the ages of 2–phase FIAs in samples where dateable minerals are spatially related to the FIAs. Because 2-phase FIAs are not present in MGSC (Fig. 3), ages of earliest MGSC precipitation provide a minimum age for the FIAs. The majority of opal that can be dated is intergrown with MGSC and the age of formation of MGSC was well constrained. The ages of primary FIAs can be constrained by dating material that is demonstrably paragenetically older and younger than a spatially related FIA. However, minerals that could be dated were commonly not spatially associated with 2-phase FIAs, limiting temporal constraints in many samples.

Nevertheless, opal and chalcedony in the older parts of some of the mineral crusts provided older constraints on the ages of 2-phase FIAs.

5.1. Results

Forty-one U-Pb and U series ages were obtained from 18 sample locations across the site (Fig. 1; Tables 2 and 3). The ages that best constrain the formation of the MGSC and the FIAs are discussed below. Additional dates and their significance, locations of the dated sample material, and detailed thin section maps are provided in the Appendix.

5.1.1. U–Pb dating of minerals in case of radioactive disequilibrium

The conventional method of calculating $^{206}Pb^*/^{238}U$ and $^{207}Pb^*/^{235}U$ isotopic ages (asterisks denote radiogenic Pb) assumes that activities of all intermediate daughter isotopes were in secular equilibrium (activities of all daughter isotopes are equal to that of the parent) at the time of mineral formation. Previous U-series studies of the Yucca Mountain opals from outermost surfaces of calcite-silica coatings revealed large initial excesses of ^{234}U and absence of ^{230}Th (Paces et al., 2000; Neymark and Paces, 2000; Neymark et al., 2000). Therefore, a more general form of the age equations for a closed system had to be applied (Bateman, 1910). Principles of U-Pb dating in case of initial radioactive disequilibrium and their application to secondary silica mineralization were discussed by Neymark et al. (2000). Equations used for the current work are applicable to systems older than 1000 years (that is, only daughter isotopes with half-lives greater than 1 yr are considered), emphasize initial disequilibrium of ^{234}U, and assume negligible initial ^{231}Pa, ^{227}Ac, ^{230}Th, ^{226}Ra, ^{210}Pb (Ludwig, 1977). The absence of these isotopes in minerals precipitated from aqueous solutions is suggested by their low solubility and short residence time in ground waters (Gascoyne, 1992), and is substantiated by very low contents of ^{232}Th and common Pb in the analyzed silica minerals (Neymark et al. 2000, 2001; Table 2).

The isotopic ratios $^{206}Pb^*/^{238}U$ and $^{207}Pb^*/^{235}U$ correspond to two independent apparent ages obtained from two different radioactive decay systems. Concordance of these ages is an important check on the closed-system behavior of the material analyzed. The age calculation from $^{206}Pb/^{238}U$ requires that the $(^{234}U/^{238}U)$ initial activity ratio must be known. Previous U-series data indicate that initial $(^{234}U/^{238}U)$ for opal and calcite from the ESF range from 2 to 10 Ma (Paces et al., 2001; Neymark and Paces, 2000). Growth of radiogenic Pb from variable excesses of ^{234}U is described by a family of concordia curves for different initial $(^{234}U/^{238}U)$, shown in Figure 10. The shape of the concordia curves reflects the fast growth of radiogenic $^{206}Pb^*$ derived from the excess ^{234}U during the first 1 m.y. after mineral deposition. Then ^{234}U reaches radioactive equilibrium with ^{238}U and the curves became parallel to each other.

In contrast to the ^{238}U decay chain, the ^{235}U decay chain contains neither daughter uranium isotopes nor any other water-soluble long-lived isotopes. The $^{207}Pb/^{235}U$ age therefore is not dependent on the unknown initial $(^{234}U/^{238}U)$. The disequilibrium $^{207}Pb/^{235}U$ ages, assuming the absence of initial ^{231}Pa and ^{227}Ac, are considered the best approximation for the timing of silica precipitation and are used in the following sections of this paper (Table 3, column d). The difference between conventional and disequilibrium $^{207}Pb/^{235}U$ ages is between 46 – 50 ka.

The $(^{234}U/^{238}U)$ and $(^{230}Th/^{238}U)$ activity ratios (Tables 2 and 3; Fig. 11) vary between ~ 1 and ~ 3.7. Young opals with $^{207}Pb/^{235}U$ disequilibrium ages less than 1.5 Ma have elevated $(^{234}U/^{238}U)$ and $(^{230}Th/^{238}U)$ ratios that are negatively correlated with the age. This is consistent

with deposition of silica from water with high ($^{234}U/^{238}U$) (Paces et al., 1998). Opal fractions with $^{207}Pb/^{235}U$ disequilibrium ages older than 1.5 – 2.0 Ma have both ($^{234}U/^{238}U$) and ($^{230}Th/^{238}U$) closer to unity. However, many of these older fractions contain small (up to 6 %, not considering two imprecise analyses) excesses of ^{234}U and ^{230}Th. This suggests relatively recent addition of uranium from the water, either by exchange between old silica and young fracture water, or, more likely, by small additional opal growth (Neymark et al. 2000; in press).

5.1.2. The role of possible multi-stage opal growth

Slightly elevated ($^{234}U/^{238}U$) and ($^{230}Th/^{238}U$) activity ratios in opals older than 1.5 – 2.0 Ma suggests mixing of small amounts of young opal with older opal. In this case the $^{207}Pb/^{235}U$ disequilibrium age would represent a minimum age of deposition for the older opal component (Neymark et al., in press). Replicate analyses of such "mixed" opals allow us to estimate the ages of the older components. Fragments of opal for replicate analyses are taken from different portions of the same opal layers, and are likely to contain variable proportions of the "old" and "young" end members. Duplicate analyses of samples ESF 27+84 Op-2, ESF 28+80 Op-2, and ESF 60+52.5 Op-1, and triplicate analysis of the sample ESF 27+84 Op-1 show variable and negatively correlated $^{207}Pb/^{235}U$ ages and ($^{234}U/^{238}U$), in agreement with two-component mixing between the "old" and "young" end members. Assuming that the "old" end member is in secular equilibrium and the end member compositions in replicate fractions are identical, we can extrapolate the ($^{234}U/^{238}U$) versus $^{207}Pb/^{235}U$ age line to ($^{234}U/^{238}U$) = 1 and get the "age of the older end member" at the axis intersection (similar for the ($^{230}Th/^{238}U$) versus $^{207}Pb/^{235}U$ age relationship). The estimated "ages of the old components" are 1.21 – 1.24 Ma for ESF 27+84 Op-2, 0.76 – 1.15 Ma for ESF 28+80 Op-2, and 1.17 – 1.26 Ma for ESF 60+52.5 Op-1. These values should be considered tentative semi-quantitative estimates, because linear extrapolation and two-component mixing are over-simplifications. Nevertheless, these estimates show that the true depositional ages of opals containing admixtures of young silica can be 0.2 – 0.7 m.y. older than their apparent $^{207}Pb/^{235}U$ ages.

Most of the studied opals have ($^{234}U/^{238}U$) and ($^{230}Th/^{238}U$) activity ratios much closer to unity than the young opals used in the above modeling. Accordingly the differences between the ages of the "old component" and the apparent $^{207}Pb/^{235}U$ ages would be smaller. The triplicate analysis of a more representative sample ESF 27+84 Op-1 yielded the estimates "age of the older end member" from 1.97 ± 0.06 to 2.05 ± 0.21 Ma, within error of the $^{207}Pb/^{235}U$ ages of 1.89-1.95 Ma. For samples older than 2 m.y. with similar or lower ($^{234}U/^{238}U$) and ($^{230}Th/^{238}U$) activity ratios, the bias in the $^{207}Pb/^{235}U$ age due to the possible presence of "young" admixture is insignificant.

5.1.3. Age of MGSC

To determine the age of MGSC, opal samples were collected from polished sections from below, within, and on top of the MGSC layer. All samples were X-ray mapped using the electron microprobe to identify MGSC and determine the paragenetic relationship between the sampled material and MGSC. The ages and the relationships between dated material and MGSC are summarized in Figure 12.

The obtained ages show that MGSC began to precipitate at Yucca Mountain between about 2.9 – 1.9 Ma. Opal collected along the boundary between bladed calcite and MGSC (ESF

72+25; Fig. 7e) gave an age of 2.90 ± 0.06 Ma, and provides a maximum age for MGSC precipitation. Opal (ESF 27+84; Fig. 7a) collected from just within MGSC near the contact between MGSC and underlying calcite provided three ages from 1.89 ± 0.09 to 1.95 ± 0.07 Ma (Table 3, column d), and indicates that MGSC began to precipitate before about 1.9 Ma. A second opal from this layer provided an age of 1.97 ± 0.04 Ma (Fig. 7a), confirming this timing. The ages determined from these two samples bracket the initial precipitation of MGSC. Additional ages, including ages younger than 1 Ma for opal from the outermost parts of crusts, show that MGSC and intergrown opal have continued to precipitate to at least within the last few hundred thousand years (Figs. 7 and 12; Appendix). A few samples of paragenetically older material consistently demonstrate that MGSC is younger than 3 – 9 Ma.

Ages determined for opal collected from the base of the MGSC in samples from other localities, for example ECRB 14 + 49 (Appendix), indicate that MGSC began to precipitate around 1.22 ± 0.02 Ma (Fig. 12, left pointing arrow at 1.0 - 1.5 Ma). This age indicates that MGSC did not start precipitating at the same time across the site and, furthermore, shows that the MGSC layer does not represent an absolute timeline. These various ages are consistent with petrographic observations and X-ray mapping that clearly show that MGSC did not precipitate in every site and that MGSC layers can vary in thickness and be discontinuous within a single sample and between adjacent samples sites (Fig. 3; Wilson and Cline, 2002). In spite of these discontinuities, the similarity in the range of ages obtained from opal associated with MGSC, as well as the distinctive chemistry and growth zoning in MGSC, permit this layer to be correlated across the site. Observations and analyses show that various sample sites recorded different components of the larger MGSC event which occurred between ~ 2.9 Ma and the last few hundred thousand years.

5.1.4. Ages of 2–phase FIAs

In some samples, calcite that precipitated before MGSC is intergrown with opal and chalcedony. Ages obtained for these samples place tighter constraints on the ages of some 2-phase FIAs. In a sample from a LC in the LCZ (Fig. 7a; ESF 27+84), primary 2–phase FIAs occur in fine mottled calcite at the base of the section. Calcite in the central part of the crust is clear and is overgrown by clear and dark MGSC. Both the central calcite and outer MGSC only contain rare liquid-only inclusions. A discontinuous clear opal layer at the boundary between the basal calcite and the central clear calcite has an age of 5.32 ± 0.02 Ma, indicating that fluids with elevated temperatures were present more than about 5.3 Ma. A discontinuous opal layer within MGSC confirmed that MGSC began to precipitate before 1.9 Ma. Opal from the outermost part of the sample gave U-Pb ages of 0.72 ± 0.42 to 0.99 ± 0.02 Ma indicating deposition of this outer layer within the last million years.

In a sample from alcove 5 (AL#5 00+28.5; Fig. 7b) in the LCZ, primary 2–phase FIAs are distributed throughout the lower and central portions of a LC crust, but are not present in outermost calcite. This youngest calcite is not MGSC and this sample does not contain the youngest mineral layer. Two-phase FIAs exhibit a clear decrease in temperature from older to younger layers in the sample. Chalcedony in the central portion of the sample gave an age of 6.29 ± 0.08 Ma, indicating that inclusions with homogenization temperatures greater than about 45 °C, which are located below this chalcedony, are older than this age. Calcite between this chalcedony and outer opal contains 2–phase FIAs that homogenize from about 37 – 43 °C. Opal paragenetically younger than these inclusions gave two ages of 5.78 ± 0.30 and 1.37 Ma showing

that these inclusions are between about 6.3 – 5.8 Ma in age. Two–phase FIAs that homogenize at 35 – 41 °C are in calcite adjacent to and outboard of the opal, and are younger than 5.8 Ma. These inclusions were the youngest 2-phase inclusions identified in this study and a minimum age for these inclusions could not be determined. However, near the outermost surface of these samples 2–phase FIAs were not observed and liquid-only inclusions are present. These liquid-only inclusions are in calcite that is older than MGSC.

A NR sample from a fracture occurrence (Fig. 7c; ESF 13+19) contains primary 2–phase FIAs with homogenization temperatures that reach 75 °C. The inclusions are in calcite adjacent to the wall rock fragments, and are overgrown by calcite, fluorite, chalcedony-quartz, and MGSC. U-Pb ages determined for chalcedony indicate that the 2–phase FIAs are older than 4.00 ± 1.46 Ma. Outer brown opal associated with MGSC has an age of 1.70 ± 0.02 Ma. Note that sparse MGSC occurs sporadically on the outermost surface of the sample and requires microprobe X-ray mapping for identification.

A sample from a shallowly dipping fracture occurrence in the LCZ contains relatively sparse 2-phase FIAs at the base and in the central part of the crust (Fig. 7d; ESF 28+80). Central calcite is overgrown by MGSC that only contains liquid-only inclusions. Two-phase FIAs near the base of the crust homogenize at temperatures of 49 – 55 °C, but other calcite that precipitated on a tuff clast contains inclusions that homogenize at 39 – 45 °C. Two-phase FIAs in the basal and central parts of the crust have generally similar homogenization temperatures between 35 – 45 °C. Opal that is younger than the 2–phase FIAs has ages between 3.29 ± 0.08 Ma and 3.88 ± 0.11 Ma, indicating that fluids with elevated temperatures were present more than about 3.9 Ma. Calcite that is not MGSC directly overlies the dated opal, confirming that MGSC is younger than 3.9 Ma. Outermost opal associated with MGSC gave ages of 0.32 ± 0.02 and 0.38 ± 0.02 Ma.

The oldest age constraint for 2–phase FIAs was obtained from a fracture occurrence in the NP (ESF 04+73.4; Fig. 7f). Several 2–phase FIAs with homogenization temperatures that reach 83 °C occur in dark calcite that is younger than basal brown opal that occurs within chalcedony, and which was dated at 9.06 ± 0.08 Ma. The dark calcite contains solid inclusions of chalcedony-quartz and is overgrown by clear calcite and MGSC that contain liquid-only inclusions. This sample indicates that the 2–phase FIAs are younger than 9 Ma and older than about 2.9 Ma. The association of chalcedony-quartz with the calcite and the light $\delta^{18}O$ composition of this calcite (~ 5 ‰; Wilson and Cline, 2002) suggest that the calcite that contains these high temperature FIAs is paragenetically early. The age of 9.06 ± 0.08 Ma is similar to ages of 7.79 ± 0.67 Ma obtained for brown opal at the base of a LC crust in the SPR (ESF 76+59.5; Appendix), and 7.94 ± 0.22 Ma obtained for chalcedony from a LC crust from the LCZ (ESF 32+31; Appendix). Two–phase FIAs with homogenization temperatures from 43 – 53 °C are present in calcite that is lateral to, but which encompasses the dated opal (Appendix). These temperatures are consistent with temperatures in older calcite.

These ages, collectively, show that 2-phase FIAs were trapped prior to 4.0 Ma, and probably prior to 5.3 Ma. The youngest identified 2-phase inclusions were trapped in calcite adjacent to and paragenetically younger than opal dated at about 5.8 Ma. These inclusions homogenize at temperatures $\leq$ 41 °C.

6. DISCUSSION

This study addressed the spatial extent and timing of the passage of fluids with elevated temperatures through the Yucca Mountain site. The presence of spatially related, liquid plus vapor fluid inclusions that provide consistent homogenization temperatures demonstrates that fluids with elevated temperatures did pass through the site. The paragenesis, microthermometry, and geochronology studies conducted as part of this project have provided the spatial relationships, temperatures, and timing of the inclusions to answer the posed questions.

Fluid inclusion petrography and microthermometry on polished sections prepared for this study and a parallel study by the USGS indicate that equivalent sections have identical paragenetic sequences but vary in mineral abundance (J. Whelan, personal communication; 2000). The parallel studies also show that fluid inclusion petrography is identical between sections, but there are variations in the abundance of 2–phase FIAs. Distribution maps for 2–phase FIAs and homogenization temperatures determined from fewer samples in a parallel study (Whelan et al., 2000) were almost identical to the data presented in this study. Earlier data collected by State of Nevada scientists (Dublyansky, 1998; Dublyansky et al. 2001) from a small number of samples are also consistent with results reported here.

Paragenesis and fluid inclusion studies indicate that fluids with elevated temperatures traveled through open spaces and precipitated secondary minerals at localities throughout the ESF and ECRB. However, secondary minerals are present in only about 10% of the available open space. The remaining 90 % contains no secondary mineral record indicating fluid flow. The secondary mineral record is a function of the amount of fluid input, porosity, permeability and connectivity of individual precipitation sites, and the time of formation of the precipitation sites relative to the fluid flux. Flow paths for early fluids may have become blocked by mineral precipitation leading to cessation of precipitation in one site and initiation of mineral precipitation in a new site. Studies of the site, however, have shown that most of the tuff is relatively porous and fluid flow through fractures and rock matrix have been demonstrated (e.g. Stuckless and Dudley, in press). Given that the rocks are porous and permeable, the general lack of secondary minerals and sparse record of fluids with elevated temperatures is most likely related to input of only small amounts of a fluid that is transporting small quantities of dissolved components.

6.1. How Widespread, Within the Repository Site, was the Influx of Fluids with Elevated Temperatures?

The passage of fluids with elevated temperatures as indicated by the presence of 2-phase FIAs is recorded in half of the secondary mineral samples collected from about 10% of the pore spaces across the ESF and ECRB. Significantly, half of the collected samples do not contain a record of these fluids, and samples that recorded the highest temperatures occur adjacent to samples that did not record elevated temperatures, or which are barren of secondary minerals. The record of elevated temperatures is more prevalent in some areas of the site (LCZ, eastern ECRB) and is sparse in other areas (SPR, western ECRB). These features show that fluids with elevated temperatures were not pervasive throughout Yucca Mountain.

The distribution of fluid temperatures is related to the timing of mineral precipitation at various sites. Where present, elevated temperatures are recorded in early to early-intermediate calcite, and the presence or absence of this record is related to whether or not early fluids with

elevated temperatures reached precipitation sites. Some of the LC that formed contemporaneously with the rock recorded the presence of higher temperature fluids. Other precipitation sites particularly fractures and breccias, probably did not exist when the earliest and highest temperature fluids were present. Fracture and breccia occurrences are interpreted to represent cooling joints and recorded the passage of later fluids with lower temperatures. The youngest calcite recorded only the presence of cool fluids, represented by liquid-only inclusions.

Variations in inclusion homogenization temperatures in the ECRB, which traverses above the potential repository horizon in the Topopah Spring Tuff, are minimal compared to the rest of the site. Petrographically the ECRB is extremely consistent; fine-grained calcite is overgrown by bladed calcite and capped by MGSC. Although many samples in the ECRB do not contain 2-phase FIAs, fluid inclusion petrography and microthermometry are similar between LC, fracture, and breccia occurrences that do. This consistency indicates a similar fluid flux across the ECRB and suggests a similar history of fluid flow for the part of the site that may host the repository.

It is noteworthy that temperatures recorded across the Yucca Mountain repository horizon do not exhibit a central hot plume and large lateral thermal gradients that are present in geothermal and epithermal systems (Henley, 1985). The lack of a significant temperature gradient and presence, instead, of relatively uniform temperatures argues against an upwelling hot fluid model.

6.2. What Temperatures do the 2–phase FIAs Represent?

Fluid inclusion petrographic and microthermometric data show that evaluated fluid inclusions comprise valid assemblages according to the criteria outlined by Goldstein and Reynolds (1994). Consistent homogenization temperatures, generally within 10 °C, show that inclusions trapped homogeneous fluids and demonstrate that the inclusions were not perturbed after they formed.

The highest temperature fluids in calcite, from about 70 – 80 °C, were only identified in the NP, in paragenetically old calcite. Fluids with temperatures reaching 70 °C were identified in the NP and NR, again in paragenetically old calcite in the welded Tiva Canyon Tuff. Interestingly no samples from the NP and NR have bimodal distributions and only recorded early fluids. Early, high temperature fluids were restricted to welded Tiva Canyon Tuff and did not extend to deeper areas. The Tiva Canyon is underlain by the PTn, an important hydrogeologic barrier that impedes downward flow as permeability changes from being fracture-controlled to matrix-controlled at the Tiva Canyon-PTn contact (e.g. Stuckless and Dudley, in press). The high temperature inclusions are found in the northeastern part of the ESF where it intersects the Tiva Canyon Tuff. High temperature fluids may have been restricted to this part of the site, or may have infiltrated Tiva Canyon Tuff elsewhere above the level of the ESF and ECRB. However, high temperature fluids were not identified in Tiva Canyon Tuff in the south portal of the ESF. The PTn tapers out between the North and South portal, and the South ramp and portal area is cut by numerous faults offsetting lithologies exposed in the ESF. High temperature fluids may not have reached this region owing to the lack of a hydrologic barrier, such as the PTn, to focus the early high temperature fluid flow along the PTn Tiva Canyon Tuff contact.

Subsequently, fluids with temperatures up to about 60 °C infiltrated the western (NR, LCZ, ECRB) and southern (SPR) part of the site. These fluids did not access the NP, suggesting that fluid flow was inhibited in this part of the site when these fluids were present. The greater abundance of silica minerals found dominantly in the NP may have reduced fluid access to this

area. These fluids also were not recorded in the IFZ because fractures had not formed at this time and there are fewer LC in this region.

As fluids cooled to less than 50 °C, fluid movement was restricted to the ECRB, LCZ, and IFZ. The majority of samples from the LCZ and ECRB recorded this lower temperature fluid plus earlier higher temperature fluids, and demonstrate fluid cooling with time (Figs. 5 and 7). Such evidence of cooling is restricted to samples from the Topopah Spring Tuff and is not observed in samples from the NP, NR, and SPR. Secondary minerals in the IFZ occur in steeply dipping fractures and recorded only cooler, < 50 °C fluids. The lack of vapor-phase mineralization, early calcite, and high temperature fluid inclusions in the IFZ support the interpretation that fractures in the IFZ formed after passage of the higher temperature fluids. Samples from this part of the ESF provide a record of intermediate and young calcite.

As more than 65 % of samples from across the site contain MGSC, the youngest, low temperature event is recorded across Yucca Mountain. Late, low temperature fluids deposited MGSC in less than 10 % of the available open space, but accessed some pore spaces across the entire site.

Rare, liquid-only inclusions are the only fluid inclusions present in outer intermediate calcite and MGSC. The presence of liquid-only inclusions has been generally accepted to indicate that the inclusions formed at < 100 °C (Roedder, 1984). However, all 2–phase and liquid-only inclusions observed in this study formed at < 100 °C. As shown in Figure 5, many 2–phase inclusions were trapped at < 50 °C. During one of the heating runs, 2–phase inclusions from the IFZ homogenized at 32 – 33 °C, below the first heating step of 35 °C, demonstrating that fluids trapped at temperatures as low as 32 °C can form 2–phase FIAs. These observations provide some of the strongest evidence that secondary minerals that contain only liquid-only fluid inclusions, which includes most intermediate calcite and MGSC, formed at temperatures below 35 °C.

The range of trapping temperatures for fluorite and quartz demonstrates that they formed over a range of temperatures at Yucca Mountain, and also shows that fluorite can precipitate at relatively low temperatures. Some homogenization temperatures from inclusions in fluorite and quartz are slightly higher than homogenization temperatures from associated calcite. The high temperatures and paragenetic positions of these minerals suggest that they formed very early, possibly during vapor phase alteration (Wilson and Cline, 2002).

Freezing point depressions for most inclusions range from -0.4 to -0.9 °C indicating a salinity range of 0.7 to 1.6 wt.% NaCl equivalent with no systematic relationship between homogenization and ice melting temperatures. These results show that regardless of fluid temperature, fluid salinity was low and inclusions may have trapped a fluid that cooled over time.

6.3. When Were 2–phase FIAs Trapped?

Paragenetic studies and fluid inclusion petrography show that 2–phase FIAs occur in early to earliest-intermediate calcite. Two-phase FIAs have not been observed in late-intermediate calcite or in outer MGSC. Therefore, based on these observations, fluids with elevated temperatures were probably not present in the recent geologic past.

Integration of fluid inclusion petrography, microthermometry and U-Pb dating establishes that elevated temperature fluids were present only during the early history of Yucca Mountain. The oldest age constraint obtained for the fluid inclusions is 9.06 ± 0.08 Ma (ESF 04+73.4; Fig.

7f), and 2–phase FIAs are younger than this age. Two-phase FIAs with temperatures > 45 °C are older than 5.32 ± 0.02 Ma (Fig. 7a), 6.29 ± 0.30 Ma (Fig. 7b), 4.00 ± 1.46 Ma (Fig. 7c), and 3.88 ± 0.11 Ma (Fig. 7d) and therefore fluids with temperatures > 45 °C were present in the site prior to 6.29 ± 0.30 Ma. Fluids with temperatures around 35 – 45 °C can be constrained to being older than 5.32 ± 0.02 Ma (Figs. 7a and b). Secondary minerals determined to be less than 5.32 ± 0.02 Ma contain only single-phase fluid inclusions and, therefore, precipitated from fluids ≤ 35 °C. Mg-enriched growth-zoned sparry calcite began to precipitate between about 2.9 and 1.9 Ma from fluids of ≤ 35 °C.

These results show that there is no fluid inclusion evidence for an influx of thermal waters into the repository site during the past 5.3 m.y. The integrated petrography, paragenetic studies, geochemistry (Wilson and Cline, 2002), fluid inclusion, and geochronological studies provides no evidence for recent hydrothermal activity.

6.4. Origin of the Fluids

The most plausible environment for secondary mineral formation is in the vadose zone (Wilson and Cline, 2002). The low δD signatures of fluid inclusion fluids (e.g. ≤ -105 ‰; Table 1) indicate that intermediate calcite and MGSC could only have been derived from meteoric fluids.

6.5. Genetic Models for the Formation of Secondary Minerals

Results presented in this paper and by Wilson and Cline (2002) are compatible with models proposed by U.S. Geological Survey geologists (Paces et al., 1996; 1998a; 1998b, 2001; Whelan et al., 1996; in press; Marshall and Whelan, 2000) that involve infiltration by descending meteoric fluids. Results are not consistent with models proposed for the formation of secondary minerals by upwelling hydrothermal fluids in the phreatic zone (Dublyansky 1998; Dublyansky et al., 1998; 2001).

U.S. Geological Survey scientists concluded that secondary minerals formed in the vadose zone and the following model is summarized from Whelan et al., (in press). A small amount of meteoric water percolated through the soils and infiltrated the UZ at Yucca Mountain. Although much of this water moved as matrix flow, some flow occurred along fracture pathways and open spaces. Highly porous vapor-phase alteration provided a pathway that diverted flow to the base of lithophysal cavities where thin water films were unevenly distributed. Water was drawn up the faces of growing crystals by surface tension, and the removal of CO_2 and H_2O via the gas phase precipitated calcite and silica (Whelan et al., in press). Fluid inclusion temperatures of 35 – 85 °C are interpreted to be common in the early stage, rare in the intermediate age, and absent in the late stage (Whelan et al., in press; Wilson et al., 2000). Early high temperatures coincided with reduced $\delta^{18}O$ compositions and cooling of the fluid with time is compatible with a progressive increase in $\delta^{18}O$ during the early and intermediate stages (Whelan et al., 2000).

6.6. Model for the Formation of Secondary Minerals

Early – early intermediate secondary minerals (> 5.32 Ma)
After deposition of the host tuff sequence and vapor-phase alteration descending meteoric fluids percolated into the warm tuff sequence (> 50 °C) and precipitated secondary minerals (calcite, quartz, fluorite) that contained 2–phase FIAs and chalcedony and brown opal in the vadose zone.

Elevated temperatures within the sequence could be expected for a few m.y. following intrusion of the Timber Mountain at around 10 Ma (Marshall and Whelan, 2000) consistent with the secondary minerals record. The NP recorded localized elevated temperatures that were not recorded in the underlying tuff units. Fluids greater than 50 °C were present at the site more than 6.29 Ma and later, cooler fluids of 35 – 45 °C were present as recently as 5.32 Ma. These temperatures indicate that the sequence was above current day ambient temperature of 27 °C for a considerable time after tuff deposition at 12.7 Ma.

Late intermediate secondary minerals (5.32 – ~2.9 Ma)

Meteoric fluids percolated into the tuff sequence at temperature less than 35 °C and temperatures within the site have not varied significantly from the present day temperature. No 2–phase FIAs were recorded in the minerals that precipitated. Only rare liquid-only inclusions were trapped. Principally calcite was deposited during this stage with rare clear opal, and very minor chalcedony-quartz. Long bladed calcite crystals formed as overgrowths on early smaller bladed calcite crystals and comprise the majority of intermediate calcite. In other sites, where space was at a premium, other calcite habits formed. δD compositions of inclusion fluids indicate formation from meteoric fluids.

Late precipitation of MGSC (~2.9 Ma to present)

The deposition of MGSC across the site was related to a change in fluid flux from that responsible for earlier secondary minerals. This change can be correlated to a climatic change in southern Nevada that resulted in cyclical increases and decreases in the Mg/Ca ratio of the meteoric fluids percolating into the site (see discussion in Wilson and Cline, 2002). MGSC precipitated from small inputs of fluids, resulting in fine Mg-enriched and depleted growth zones. Precipitation by small fluid inputs is supported by ages determined for this layer that confirm minimal or no precipitation over a significant period of time. Rare liquid-only inclusions are consistent with MGSC forming from thin films of fluid and indicate that MGSC formed at < 35 °C. The presence of MGSC across the site suggests that the processes responsible for formation of this calcite occurred across the site and that the site has been stable, on conservative estimates, for the last few million years.

7. CONCLUSIONS

Two-phase FIAs indicative of elevated temperatures are present in secondary mineral crusts at the proposed Yucca Mountain nuclear waste repository. These 2–phase FIAs occur predominantly in paragenetically early calcite around the wall rock at the base of mineral crusts. Rare 2–phase FIAs occur in the earliest intermediate minerals but they are not present in late intermediate calcite and the youngest Mg-enriched growth zoned sparry calcite (MGSC). Only rare liquid-only inclusions are present in late intermediate minerals and outer MGSC.

Homogenization temperatures obtained from calcite across the site are 35 – 83 °C. Rare fluorite and quartz contain 2–phase FIAs that typically had homogenization temperatures similar to adjacent calcite. The majority of samples across the site recorded fluids of 45 – 60 °C. Some calcite from the North portal formed at higher temperatures than calcite elsewhere, and recorded fluid temperatures up to 83 °C in one sample. These localized high temperatures were also recorded by 2–phase FIAs in quartz and fluorite. Samples from the IFZ recorded cooler

temperatures of 40 – 50 °C. The majority of samples collected from the Topopah Spring Tuff, mainly from LC occurrences, indicate a cooling trend with time; homogenization temperatures at the base of the crusts formed at temperatures > 50 °C and paragenetically younger basal calcite formed at temperatures of 35 – 45 °C. The timing relationships suggest that the 35 – 45 °C inclusions are equivalent to the low temperature 2–phase FIAs observed in the IFZ. Only rare liquid-only inclusions are observed in paragenetically younger calcite. The presence of liquid-only FIAs indicates that young secondary minerals formed at temperatures less that 35 °C. Freezing point depressions of -0.2 to -1.6 °C (mode -0.4 to -0.9 °C) are consistent with formation from a low salinity fluid and suggest that secondary minerals formed from similar fluids.

Integration of fluid inclusion petrography and microthermometry with U-Pb dating indicates that fluids with elevated temperatures have not been present in the recent geologic past. Two-phase FIAs adjacent to the wall rock that trapped fluids of > 50 °C are older than 6.29 ± 0.30 Ma. Two-phase FIAs in paragenetically later, early calcite which formed from fluids of 35 – 45 °C are older than 5.32 ± 0.02 Ma. The consistent homogenization temperatures obtained for 2-phase FIAs in early minerals argues strongly that the site has not been perturbed since these fluid inclusions were trapped. There is no evidence of fluids with elevated temperatures in secondary minerals that formed during the past 5.32 m.y. The presence of MGSC across the site indicates a consistent flux from ambient temperature fluids during the past 2 to 3 m.y.

Results from this study are not consistent with models requiring formation of secondary minerals in a saturated environment at Yucca Mountain. Results, furthermore, provide no evidence for the former presence of upwelling hydrothermal fluids. Alternatively, results are consistent with infiltration of a cooling tuff sequence by descending meteoric water. This study demonstrates that the hypothesis of geologically recent upwelling hydrothermal fluids is untenable and should not disqualify Yucca Mountain as a potential nuclear waste storage site.

Acknowledgements. We would like to thank Drew Coleman (DOE-YMP) for his help during all aspects of this project, Joel Rotert for assistance during sampling and for hours of patient microthermometry, and Bob Bodnar for his technical review of this report. Bob Bodnar, Yuri Dublyanski, Bob Goldstein, Ed Roedder, Joe Whelan and Ike Winograd are thanked for discussions on all aspects of this project. Project funding was awarded to JSC under DOE Cooperative Agreement DE-FC08-98NV-12081.

All data presented in this report were collected under the University and Community College System of Nevada (UCCSN) Quality Assurance Program. Technical Data Managment System data tracking number UN0203SPA004JC.001 correlates to data collected during this study. Access to electronic data was limited to task personnel and controlled with the use of passwords. Loss was prevented by use of backup files. Manual entry and file transfers were verified for accuracy. No electronic data were lost or corrupted.

REFERENCES

Bateman H. (1910) Solution of a system of differential equations occurring in the theory of radio-active transformations. Proc. Cambridge Phil. Soc. 15, 423-427.

Bish D. L. and Aronson J. L. (1993) Paleogeothermal and paleohydrologic conditions in silicic tuff from Yucca Mountain, Nevada. *Clays and Clay Minerals*, **41**, 2, p. 148-161.

Bodnar R. J. (1993) Revised equation and table for determining the freezing point depression of H_2O-NaCl solutions. *Geochim. Cosmochim. Acta*, **57**, 683-684.

Buesch D. C., Spengler R. W., Moyer T. C. and Geslin J. K. (1996) Proposed stratigraphic nomenclature and macroscopic identification of lithostratigraphic units of the Paintbrush Group exposed at Yucca Mountain, Nevada. U. S. Geological Survey Open-File Report 94-469, 47 p.

Carlos B. A. (1994) Field guide to fracture-lining minerals at Yucca Mountain. Los Alamos National Lab. Rep. LA-12803-MS.

Christiansen R. L, Lipman P. W., Carr W. J., Byers F. M Jr., Orkild P. P. and Sargent K. A. (1977) Timber Mountain-Oasis Valley caldera complex of southern Nevada. *GSA Bulletin* **88**, 943-959.

Data Tracking Number UN0203SPA004JC.001. Thermochronological evolution of calcite formation at Yucca Mountain. Submittal date: 03/26/2002.

Dublyansky Y. (1998) Fluid inclusion studies of samples from the Exploratory Study Facility, Yucca Mountain, Nevada. Institute for Energy and Environmental Research, Washington.

Dublyansky Y., Szymanski J., Chepizhko A., Lapin B. and Reutsky V. (1998) Geological history of Yucca Mountain (Nevada) and the problem of a high-level nuclear waste repository. In *Defense Nuclear Waste Disposal in Russia* (eds. M. Stenhouse and V. Kirko). NATO Series, Kluwer Academic Publishing, Netherlands, pp. 279-292.

Dublyansky Y., Ford D. and Reutski V. (2001) Traces of epigenetic hydrothermal activity at Yucca Mountain, Nevada: preliminary data on the fluid inclusion and stable isotope evidence. *Chemical Geology* **173**, 125-149.

Gascoyne M. (1992) Geochemistry of actinides and their daughters. In *Uranium-series Disequilibrium: Applications to Earth, Marine, and Environmental Sciences, 2nd ed.*, Clarendon Press.

Goldstein R. H. and Reynolds T. J. (1994) Systematics of Fluid Inclusions in Diagenetic Minerals, SEPM Short Course 31, Tulsa, Oklahoma, 199 p.

Heizler M. T., Perry F. V., Crowe B. M., Peters L. and Appelt R. (1999) The age of the Lathrop Wells volcanic center: an $^{40}Ar/^{39}Ar$ dating investigation. *Jour. Geophy. Res.* **104**, 767-804.

Henley, R.W. (1985) The geothermal framework of epithermal deposits. In *Geology and Geochemistry of Epithermal Systems, Reviews in Economic Geology, Vol. 2,* B.R. Berger and P.M. Bethke (eds.), 1-24.

Lawler and Crawford (1983) Stretching of fluid inclusions resulting from a low temperature microthermometric technique. *Economic Geology* **78,** 527-529.

Levy, S., Norman D. and Chipera S. (1996) Alteration History Studies in the Exploratory Studies Facility, Yucca Mountain, Nevada, USA. In *Scientific Basis for Nuclear Waste Management XIX*, W. Murphy and D. Knecht (eds.), 783-790.

Ludwig K. R. (1977) Effect of initial radioactive-daughter disequilibrium on U-Pb isotope apparent ages of young minerals. *J. Res. U. S. Geol. Survey* **5**, 663-667.

Ludwig K. R., Wallace A. R., and Simmons K. R. (1985) The Schwartzwalder uranium deposit, II: Age of uranium mineralization and lead isotope constraints on genesis. *Economic Geology* **80**, 1858-1871.

Marshall B. D. and Whelan, J.F. (2000) Isotope geochemistry of calcite coatings and the thermal history of the unsaturated zone at Yucca Mountain, Nevada. GSA annual meeting, Nov. 13-16. Reno, Nevada, *Abstracts with Programs, T111,* A-259.

Neymark L. A. and Paces J. B. (1996) Mixed isotopic ages as a consequence of very slow rates of deposition in Quaternary subsurface fracture-coatings, GSA annual meeting, Oct. 28-31. Denver, Colorado, *Abstracts with Programs, 28, N7*, A139.

Neymark L. A. and Paces J. B. (2000) Consequences of slow growth for ^{230}Th/U dating of Quaternary opals, Yucca Mountain, Nevada, USA. *Chem. Geol.* **164**, 143-160.

Neymark L. A., Paces J. B and Amelin Y. V. (1998) Neogene to Quaternary U-Th-Pb geochronology using opal, Yucca Mountain, Nevada, USA. *Mineral. Mag.* **62A**, 1077-1078.

Neymark L. A., Amelin Y. A. and Paces J. B. (2000) ^{206}Pb-^{230}Th-^{234}U-^{238}U and ^{207}Pb-^{235}U geochronology of Quaternary opal, Yucca Mountain, Nevada. *Geochim. Cosmochim. Acta* **64**, 2913-2928.

Neymark L.A., Amelin Y., Paces J.B., Peterman Z.E. U-Pb ages of secondary silica and implications for paleohydrology of the unsaturated zone at Yucca Mountain, Nevada. *Applied Geochemistry*, in press.

Paces J. B., Neymark L. A., Kwak L. M., and Peterman Z. E. (1996) U-series dating of secondary minerals as a tool for estimating paleo water flux through a thick unsaturated zone, Yucca Mountain, NV, GSA Annual meeting, October 28-31, Denver, Colorado, *Abstracts with programs*, A139-A140 (abstr.).

Paces J. B., Marshall. B. D., Whelan, J. F. and Neymark L. A. (1997) Progress Report on Unsaturated Zone Stable and Radiogenic Isotope Studies, U.S. Geological Survey Milestone report SPC23FM4.

Paces J. B., Neymark L. A., Marshall B. D., Whelan J. F. and Peterman Z . E. (1998a) Inferences for Yucca Mountain unsaturated zone hydrology from secondary minerals. *Proc., Intl. High-Level Rad. Waste Manag. Conf., Las Vegas, NV, May 11-14, 1998,* Amer. Nucl. Soc., 36-39.

Paces J. B., Ludwig K. R., Peterman Z. E., Neymark L. A., and Kenneally J. M. (1998b) Anomalous ground-water ^{234}U/^{238}U beneath Yucca Mountain: Evidence of local recharge? *Proc., Intl. High-Level Rad. Waste Manag. Conf., Las Vegas, NV, May 11-14, 1998,* Amer. Nucl. Soc., 185-188.

Paces J.B., Neymark L.A., Persing H. M. and Wooden, J. L. (2000) Demonstrating slow growth rates in opal from Yucca Mountain, Nevada, using microdigestion and ion-probe uranium-series dating. Geological Society of America Abstracts with Programs, vol. 32, p. A-259 (abst.).

Paces J. B., Neymark, L. A., Marshall, B. D., Whelan J. F. and Peterman Z. E. (2001) Ages and origins of calcite and opal in the Exploratory Studies Facility Tunnel, Yucca Mountain, Nevada. U.S. Geological Survey, Water-Resources Investigations Report 01-4049, Denver, CO, 95 p.

Roedder, E., 1984, Fluid Inclusions, Reviews in Mineralogy Volume 12: Mineralogical Society of America, VPI&SU, Blacksburg, Virginia, 644 p.

Roedder, E. and Bodnar, R. (1980) Geologic pressure determinations from fluid inclusion studies. *Annual Review Earth and Planetary Sciences* **8,** 263-301.

Roedder E. and Whelan J. F. (1998) Ascending or descending water flow through Yucca Mountain tuffs? Fluid inclusion evidence. In *PACROFI VII; Pan-American conference on Research on fluid inclusions program and abstracts* (eds. D. A. Vanko and Cline J. S.) p. 56.

Roedder E., Whelan J. F. and Vaniman, D. T. (1994) Fluid inclusion crushing and homogenization studies of calcite veins from Yucca Mountain, Nevada, tuffs; environment of formation, In *International Mineralogical Association, 16th general meeting abstracts,* p. 354-355.

Sawyer D. A., Fleck R. J., Lanphere M. A., Warren R. G., Broxton D. E. and Hudson M. R. (1994) Episodic Caldera Volcanism in the Miocene Southwestern Nevada Volcanic Field: Revised Stratigraphic Framework, $^{40}Ar/^{39}Ar$ Geochronology, and Implications for Magmatism and Extension. *GSA Bulletin* **106**, 1304-1318.

Sharp Z. D., Atudorei V. and Durakiewicz, T. (2001) A rapid method for determination of hydrogen and oxygen isotope ratios from water and hydrous minerals. *Chemical Geology* **178**, 197-210.

Stewart J. H (1988) Tectonics of the Walker Lane Belt, Western Great Basin – Mesozoic and Cenozoic Deformation in a Zone of Shear. In *Metamorphism and crustal evolution of the western United States* (ed. W. G. Ernst), Vol. VII, Prentice-Hall Inc., New Jersey, p. 684-713.

Stuckless J. S. and Dudley W. W. (2002) The Geohydrologic Setting of Yucca Mountain, Nevada. *Applied Geochemistry, in press.*

Szymanski J. S. (1987) Conceptual Considerations of the Death Valley Groundwater System with Special Emphasis on the Adequacy of This System to Accommodate the High-Level Nuclear Waste Repository (draft). *DOE internal report*, Yucca Mountain Project Office, Las Vegas Nevada, Nov. 1987.

Szymanski J. S. (1989) Conceptual Considerations of the Yucca Mountain Groundwater System with Special Emphasis on the Adequacy of This System to Accommodate the High-Level Nuclear Waste Repository. *DOE internal report*, Yucca Mountain Project Office, Las Vegas Nevada, July 1989.

U.S. Department of Energy (1988) Site characterization plan, Yucca Mountain site, Nevada research and development area, Nevada. U.S. Dept. Energy Report, DOE/RW-0199-8 Volumes.

Whelan J. F., Moscati R. J., Allerton S. B. M. and Marshall. B. D. (1996) Applications of isotope geochemistry to the reconstruction of Yucca Mountain, Nevada, Paleohydrology – status of investigations. U.S. Geological Survey, Open-file report 98-83.

Whelan J. F., Paces J. B., Neymark L. A. and Peterman, Z. E. (2000) Status of fluid inclusion studies, U.S. Geological Survey, Water-Resource Investigation Status Report, 8191213UU5.

Whelan J. F., Paces J. B. and Peterman Z. E. (2002) Paragenetic Relations and Evidence for Secondary Mineral Formation in Unsaturated-zone Tuffs at Yucca Mountain, Nevada. *Applied Geochemistry, in press.*

Wilson N. S. F., Cline J. S., Rotert J. and Amelin Y. A. (2000) Timing and Temperature of Fluid Movement at Yucca Mountain, NV: Fluid inclusion and U-Pb and U-series dating, GSA Annual meeting, Nov. 13-16, Reno, Nevada, *Abstracts with programs*, A-260 (abstr.).

Wilson N. S. F. and Cline J. S. (2002) Thermochronological evolution of calcite formation at the potential Yucca Mountain repository site, Nevada: Part 1, Secondary mineral paragenesis and geochemistry. *Companion report submitted to DOE.*

Winograd I. J. (1981) Radioactive waste disposal in thick unsaturated zones. *Science* **212**, 1457-1464.

FIGURE CAPTIONS

Figure 1 Sample locations in the ESF, ECRB, and exploratory alcoves. Circles mark sample locations; filled circles indicate samples that contained 2–phase FIAs. Arrows point to samples that were dated. The site has been divided into six regions that are labeled and discussed in the text.

Figure 2 $^{230}Th/^{238}U$ and $^{234}U/^{238}U$ activity ratios in the in-house secular equilibrium standard SU-1 (Schwartzwalder uranium ore, Ludwig et al. 1985, see also Neymark et al. 2000), analyzed with the Yucca Mountain samples during the period of June to December 2000. The x-axis is equivalent to time with respect to the analyses.

Figure 3 Schematic diagram illustrating the mineral paragenesis and spatial distribution of 2–phase FIAs in secondary mineral crusts at Yucca Mountain (adapted from Wilson and Cline, 2002). Basal calcite and the central early cores of the bladed calcite, just above the qtz-cdy layer, are considered early to early-intermediate. The left side of the figure shows the typical paragenesis for fracture and breccia samples, whereas the rest of the figure illustrates the variability in parageneses in lithophysal cavities. See text for discussion. Cdy is chalcedony, Td is tridymite, Hem is hematite, and Qtz is quartz.

Figure 4 Fluid inclusion populations, distinguished by arrow color, under plane polarized light. Two–phase fluid inclusions are shown by black arrows, liquid-only inclusions are shown by white arrows, and 2–phase inclusions with inconsistent liquid-vapor ratios are indicated by gray arrows. **(A)** Typical primary liquid-only FIA in bladed calcite. **(B)** Primary all-liquid FIA along a growth zone in MGSC. No 2–phase FIAs have been observed in this outermost calcite. **(C)** Primary 2–phase FIA along a growth zone at the base of a LC. Microthermometry gave consistent homogenization temperatures of 43 – 53 °C (n = 43). **(D)** Primary (?) assemblage of 2–phase fluid inclusions with consistent liquid-vapor ratios and homogenization temperatures (53 – 59 °C; n = 23). Two-phase FIAs include liquid-only inclusions, 2–phase inclusions with variable liquid-vapor ratios, and vapor-only inclusions.

Figure 5 Summary of fluid inclusion homogenization temperatures for six areas (Fig. 1) in the ESF and ECRB. The vertical dashed line represents a reference temperature of 50 °C. Note the consistency of data within each of the six areas and the differences in homogenization temperatures between areas. In samples with two modes, higher homogenization temperatures were obtained from paragenetically older calcite and lower homogenization temperatures from paragenetically younger calcite, indicating a cooling trend with time. See text for discussion.

Figure 6 Histogram of fluid inclusion homogenization temperatures obtained from sample ESF 01+62.3 near the north portal from the welded Tiva Canyon tuff. These data were collected from 2 sample chips with the summarized data from the first chip

shown in white. Individual assemblages from the second chip have similar ranges and data are similar to the summarized data. In some assemblages (3 and 6) only a few inclusions were chosen (at random) and measured from larger FIAs. This was done to see how many inclusions were required to produce a valid distribution of data for the entire FIA. Assemblages 3 and 6 have modes and distributions similar to the larger data set and indicate that not all inclusions must be measured to obtain representative data for the samples.

Figure 7 Doubly polished sections showing the locations of primary 2–phase FIAs (black squares) and the locations of opal and chalcedony dated using U-Pb methods. Yellow filled squares indicate 2-phase FIAs that were examined using microthermometry. Homogenization temperatures are given adjacent to the squares. Opal and chalcedony are shown in black with dated areas indicated in red; ages and errors are shown adjacent to the dated material. All dated material was opal unless stated. Dashed black lines indicate the boundaries between MGSC and underlying secondary minerals. (A) Two–phase FIAs are located below, and are older than, the 5.32 $\pm$ 0.02 Ma opal layer (gray). Only liquid-only inclusions occur above this layer in intermediate calcite and outer MGSC. An outer discontinuous opal layer (dashed blue line) was precipitated within the MGSC layer. (B) Lithophysal cavity crust from the LCZ. Two–phase FIAs occur throughout most of the crust and vary from 45 – 57 °C at the base of the sample to 35 – 41 °C near the outer part of the sample. Dates on chalcedony near the center of the crust indicate that 2–phase FIAs with homogenization temperatures of 45 – 57 °C are older than 6.29 $\pm$ 0.08 Ma. Opal near the outer part of the crust was dated at 5.78 $\pm$ 0.3 Ma and 35 – 41°C 2–phase FIAs are younger than this age. MGSC does not occur on the outermost surface indicating that young secondary minerals did not precipitate at this location. The locations of 2–phase FIAs are only shown for the left side of the section in basal calcite below the 6.29 $\pm$ 0.08 Ma chalcedony, but 2–phase FIAs are present in the basal calcite across the section. All 2–phase FIAs observed in the outer part of the crust are shown. (C) Crust from a fracture occurrence in the NR. Primary 2–phase FIAs have homogenization temperatures of 67 – 75 °C and are older than 4.00 $\pm$ 1.46 Ma, the age of a chalcedony layer that is younger than the primary 2–phase FIAs. A younger brown opal layer associated with MGSC has an age of 1.70 $\pm$ 0.02 Ma. (D) Shallowly dipping fracture sample from the LCZ. Three ages determined for opal (Table 3, column d) indicate that 2–phase FIAs are older than 3.88 $\pm$ 0.11 Ma. (E) Lithophysal cavity crust with bladed calcite overlain by MGSC associated with opal. No 2–phase FIAs are present in this sample but opal occurs along the boundary between bladed calcite and outer MGSC and indicates that MGSC formed after 2.90 $\pm$ 0.06 Ma. (F) Lithophysal cavity crust with chalcedony with brown opal patches that have an age of 9.06 $\pm$ 0.09 Ma overlain by dark calcite that contains abundant 2–phase FIAs. This calcite is overgrown by a thin layer of younger calcite and outer layer of MGSC that contains rare liquid-only inclusions. In this sample the 2–phase FIAs, with homogenization temperatures from 69 – 83 °C, are younger than 9.06 $\pm$ 0.09 Ma. $\delta^{18}O$ compositions are

consistent with this calcite forming early and at higher temperature (Wilson and Cline, 2002).

Figure 8 Homogenization temperatures from fluorite and quartz. All data were obtained from paragenetically early fluorite and quartz that precipitated around and adjacent to the host tuffs. Homogenization temperatures for fluorite vary from 43 – 91 °C and for quartz from 53 – 95 °C. Homogenization temperatures for fluorite and quartz vary across the site and samples from the NP have higher homogenization temperatures than samples from other areas. Homogenization temperatures obtained for fluorite and quartz are generally similar to homogenization temperatures obtained from adjacent secondary minerals where present.

Figure 9 Histogram of ice melting temperatures (n = 129) for fluid inclusions in calcite (n = 127) and fluorite (n = 2; Tm = -0.7 °C) from 30 samples across the site.

Figure 10 U-Pb concordia diagram for opals. Common-lead-corrected $^{206}Pb/^{238}U$ and $^{207}Pb/^{235}U$ ratios for Yucca Mountain opals are plotted together with concordia curves corresponding to $^{234}U/^{238}U$ initial activity ratios (U_i) of 1, 3 and 10. Isochrons are shown as vertical dotted lines connecting points of equal age on the concordia curves. It is assumed that initial ^{230}Th, ^{231}Pa, and ^{227}Ac are absent. Error ellipses are 2 σ. The distribution of the data indicates variations of $^{234}U/^{238}U$ initial activity ratios between values 1 and > 10 (values are shown in Table 3).

Figure 11 Measured $^{234}U/^{238}U$ **(A)** and $^{230}Th/^{238}U$ **(B)** activity ratios versus $^{207}Pb/^{235}U$ disequilibrium ages in Yucca Mountain opals. Error bars are 2 σ. Analytical points for three very young opal fractions with $^{234}U/^{238}U_{activity}>2$ are not shown.

Figure 12 Histogram of U-Pb ages obtained from opal (open squares) and chalcedony (filled squares). Arrows indicate the location of the dated sample within the section with respect to MGSC. Arrows pointing right indicate that the dated sample was collected from material paragenetically younger than MGSC; double arrows indicate that the dated sample was collected from within MGSC, and arrows pointing left indicate that the dated sample was collected from material paragenetically older than MGSC. The shaded bar indicates the approximate time of initial precipitation of MGSC. See text for discussion.

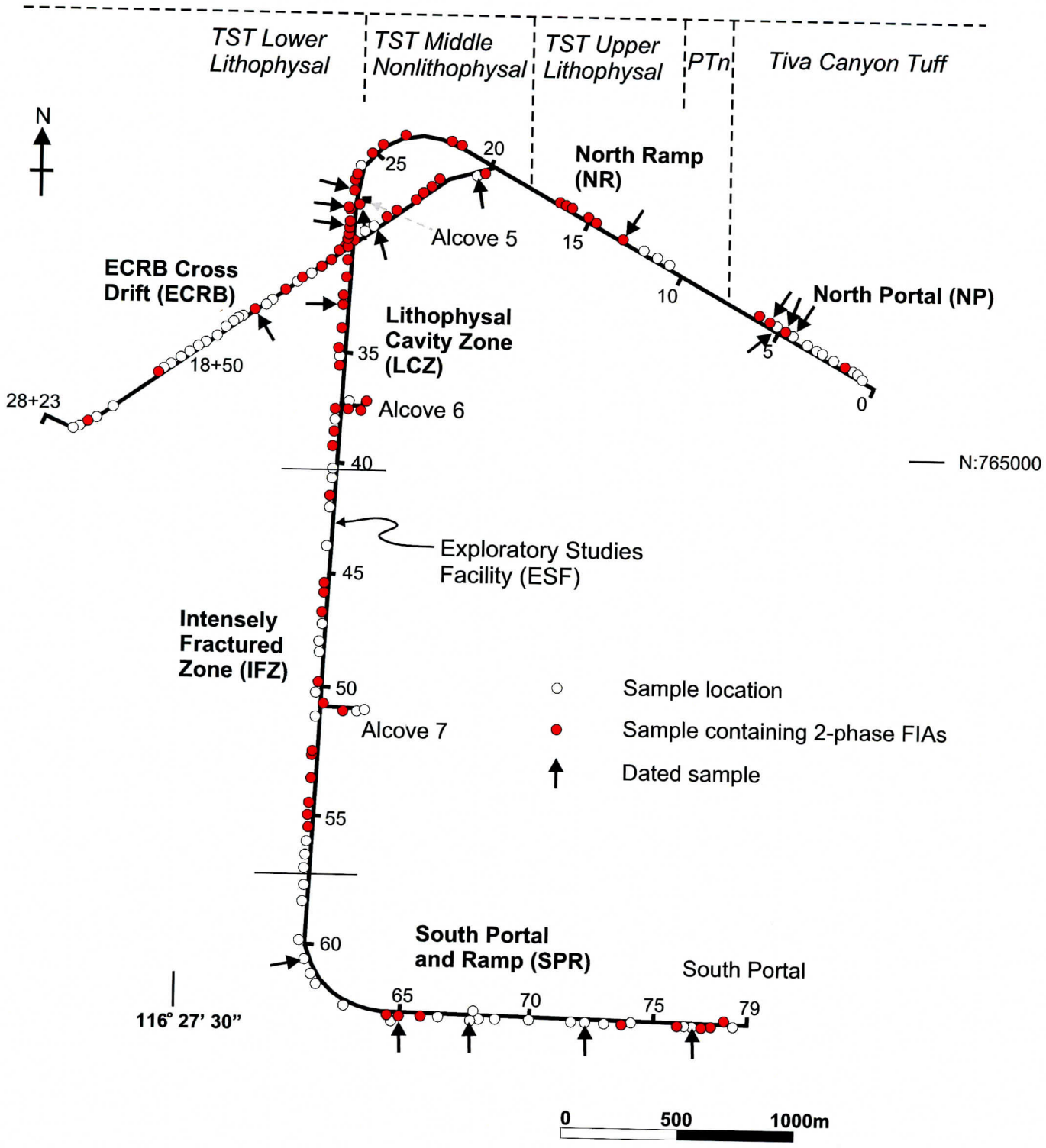
TST Lower Lithophysal
TST Middle Nonlithophysal
TST Upper Lithophysal
PTn
Tiva Canyon Tuff
N
North Ramp (NR)
Alcove 5
ECRB Cross Drift (ECRB)
Lithophysal Cavity Zone (LCZ)
North Portal (NP)
Alcove 6
N:765000
Exploratory Studies Facility (ESF)
Intensely Fractured Zone (IFZ)
Sample location
Sample containing 2-phase FIAs
Dated sample
Alcove 7
South Portal and Ramp (SPR)
South Portal
116° 27' 30"
0
500
1000m

Figure 1

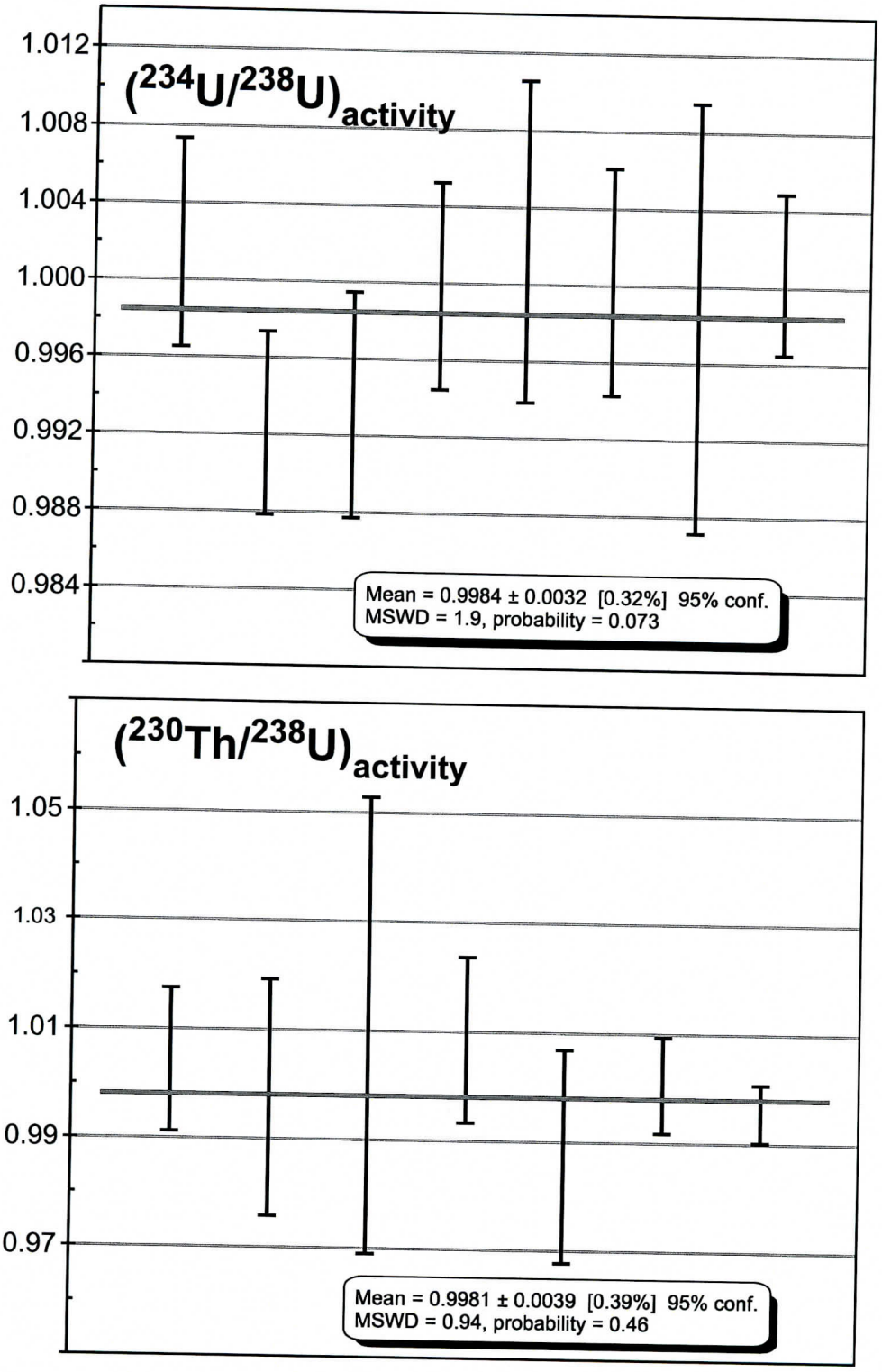
1.012
1.008
1.004
1.000
0.996
0.992
0.988
0.984
(234U/238U)activity
Mean = 0.9984 ± 0.0032 [0.32%] 95% conf.
MSWD = 1.9, probability = 0.073
(230Th/238U)activity
1.05
1.03
1.01
0.99
0.97
Mean = 0.9981 ± 0.0039 [0.39%] 95% conf.
MSWD = 0.94, probability = 0.46

Figure 2

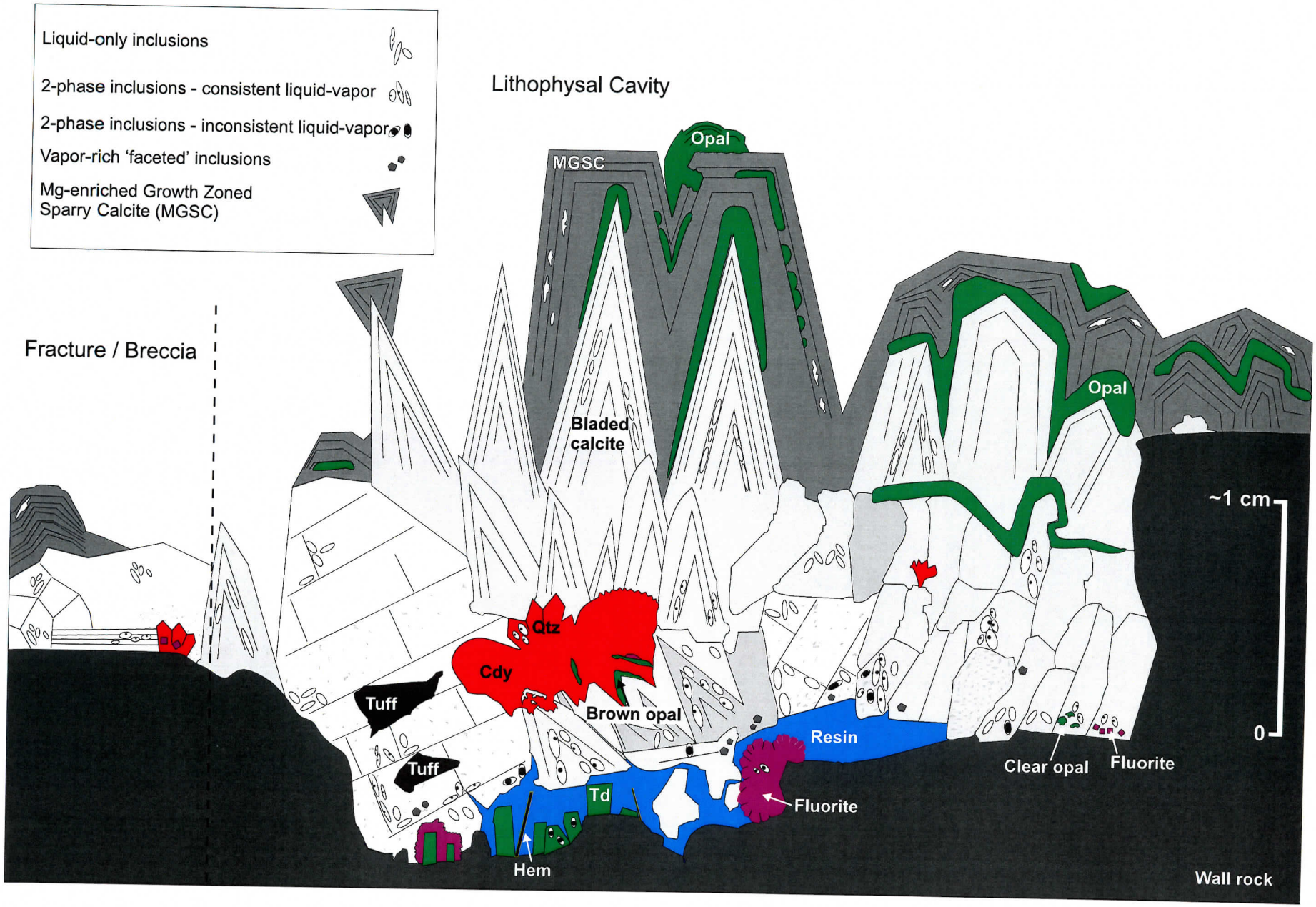
Liquid-only inclusions
2-phase inclusions - consistent liquid-vapor
2-phase inclusions - inconsistent liquid-vapor
Vapor-rich 'faceted' inclusions
Mg-enriched Growth Zoned Sparry Calcite (MGSC)
Lithophysal Cavity
Fracture / Breccia
Opal
MGSC
Bladed calcite
Opal
~1 cm
0
Qtz
Cdy
Tuff
Brown opal
Resin
Tuff
Td
Fluorite
Clear opal
Fluorite
Hem
Wall rock

Figure 3

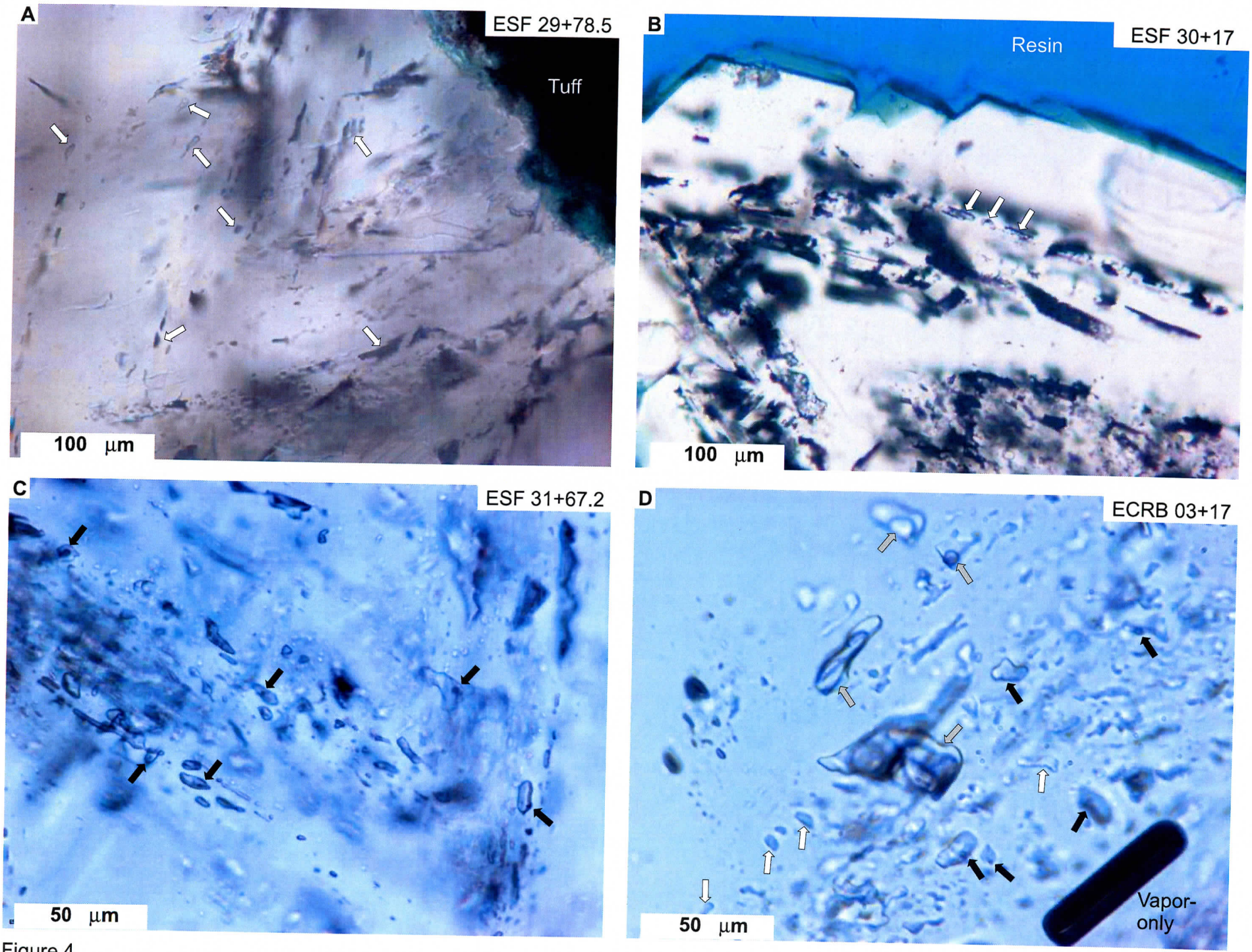
A
ESF 29+78.5
Tuff
100 µm
B
Resin
ESF 30+17
100 µm
C
ESF 31+67.2
50 µm
D
ECRB 03+17
Vapor-
only
50 µm

Figure 4

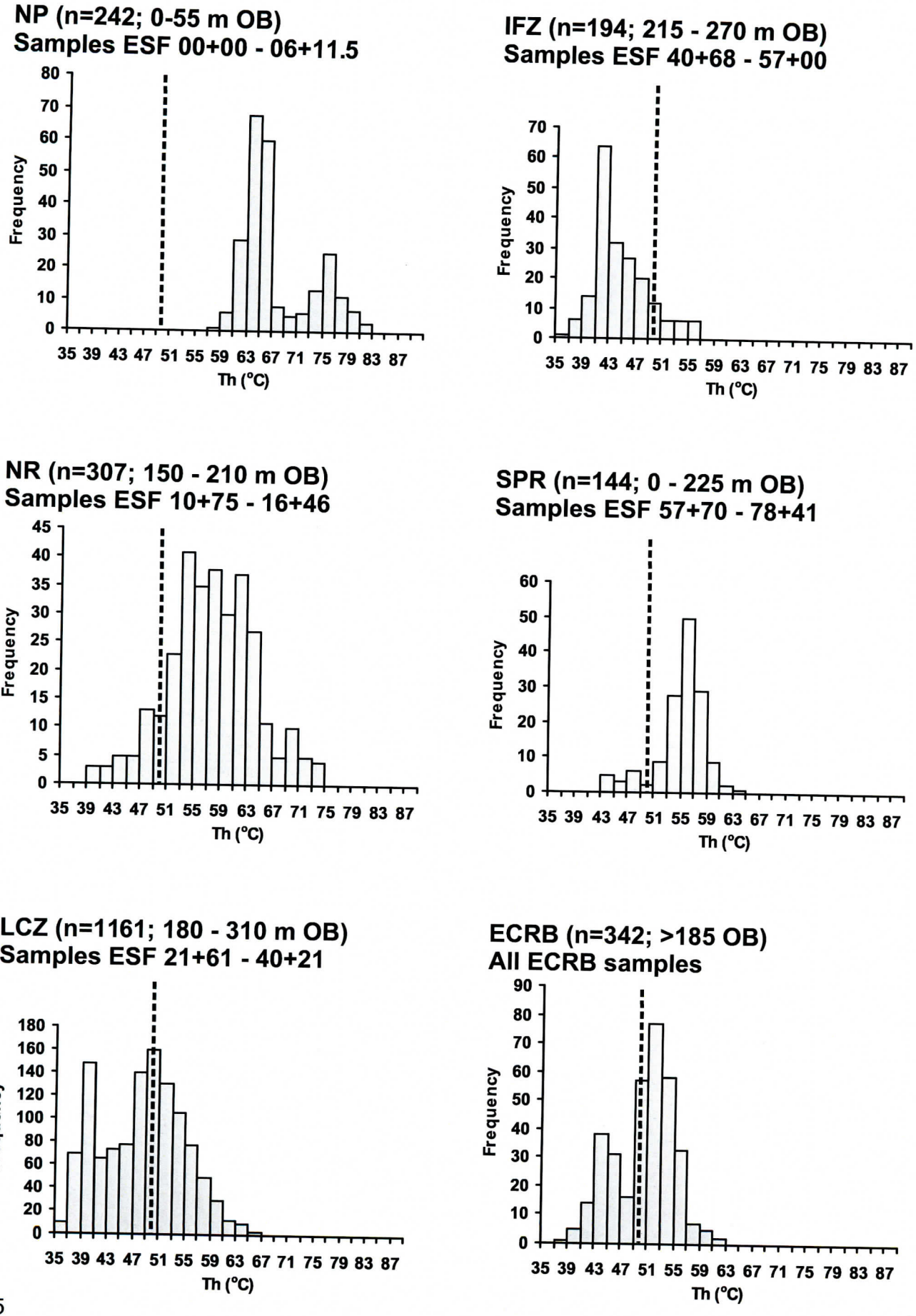
NP (n=242; 0-55 m OB)
Samples ESF 00+00 - 06+11.5
Frequency
Th (°C)
IFZ (n=194; 215 - 270 m OB)
Samples ESF 40+68 - 57+00
Frequency
Th (°C)
NR (n=307; 150 - 210 m OB)
Samples ESF 10+75 - 16+46
Frequency
Th (°C)
SPR (n=144; 0 - 225 m OB)
Samples ESF 57+70 - 78+41
Frequency
Th (°C)
LCZ (n=1161; 180 - 310 m OB)
Samples ESF 21+61 - 40+21
Frequency
Th (°C)
ECRB (n=342; >185 OB)
All ECRB samples
Frequency
Th (°C)

Figure 5

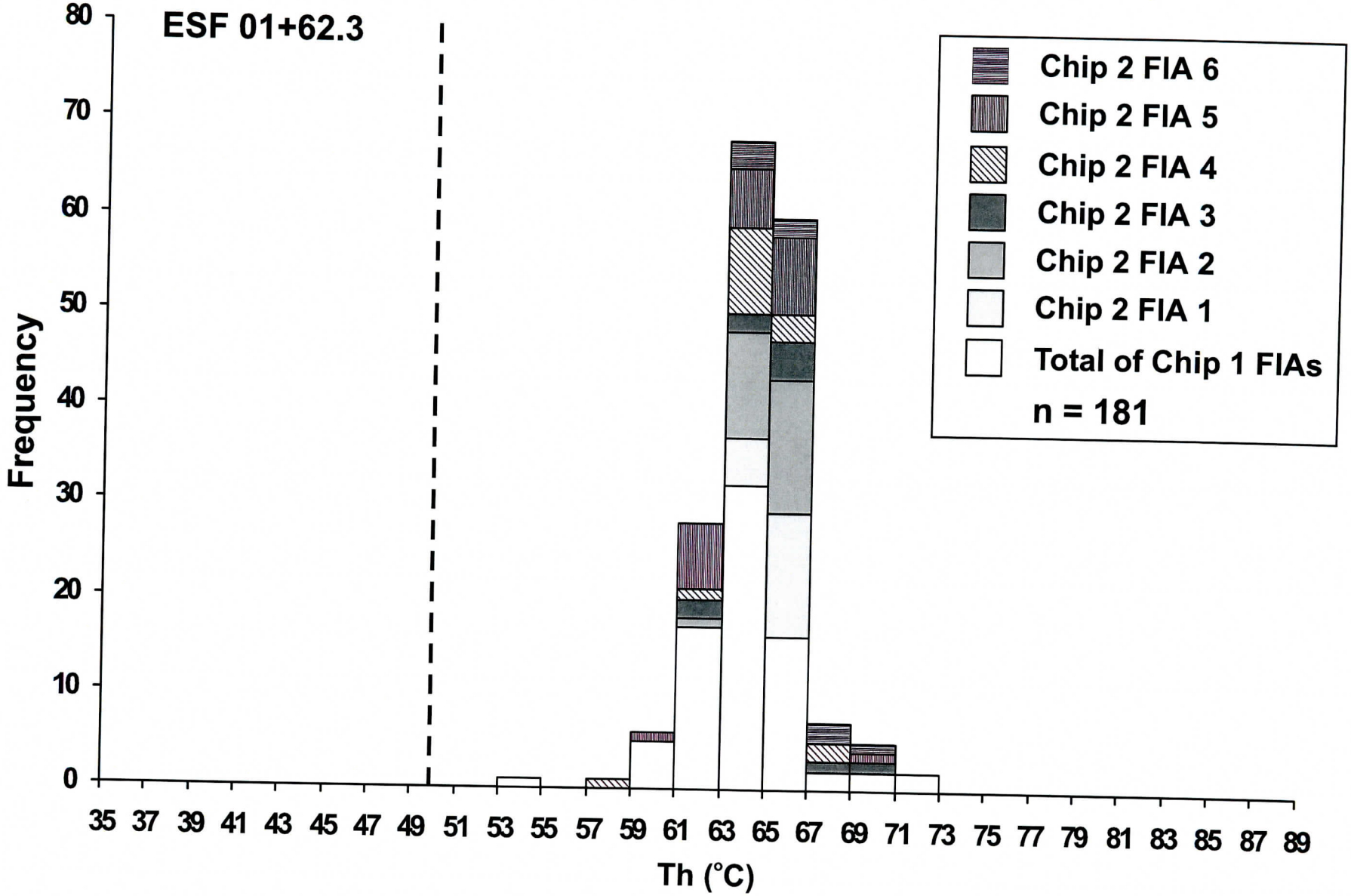
ESF 01+62.3
Chip 2 FIA 6
Chip 2 FIA 5
Chip 2 FIA 4
Chip 2 FIA 3
Chip 2 FIA 2
Chip 2 FIA 1
Total of Chip 1 FIAs
n = 181
Frequency
0
10
20
30
40
50
60
70
80
35 37 39 41 43 45 47 49 51 53 55 57 59 61 63 65 67 69 71 73 75 77 79 81 83 85 87 89
Th (°C)

Figure 6

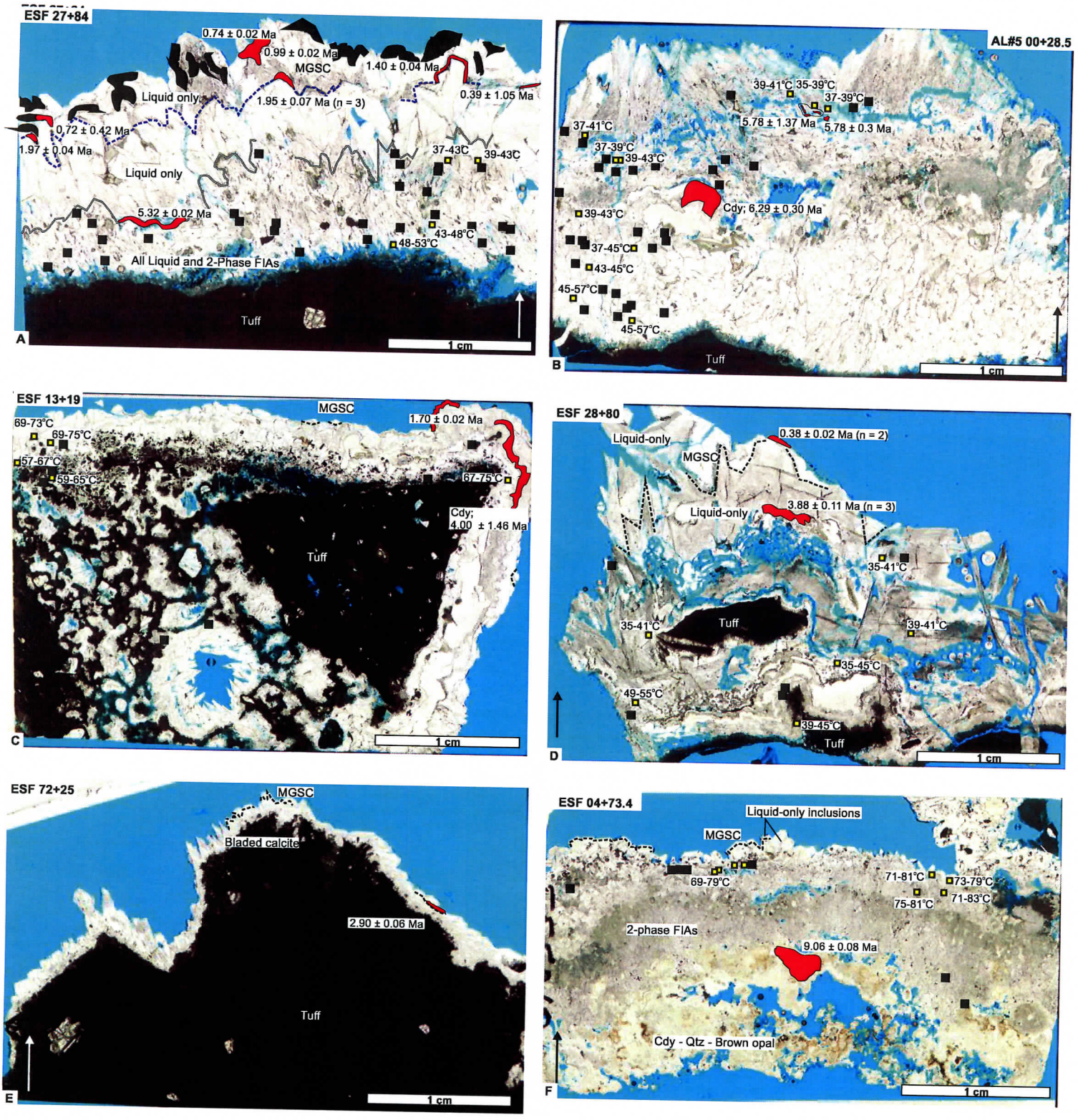
ESF 27+84
0.74 ± 0.02 Ma
0.99 ± 0.02 Ma
MGSC
1.40 ± 0.04 Ma
Liquid only
1.95 ± 0.07 Ma (n = 3)
0.39 ± 1.05 Ma
0.72 ± 0.42 Ma
1.97 ± 0.04 Ma
37-43°C
39-43°C
Liquid only
5.32 ± 0.02 Ma
43-48°C
48-53°C
All Liquid and 2-Phase FIAs
Tuff
1 cm
A
AL#5 00+28.5
39-41°C
35-39°C
37-39°C
37-41°C
5.78 ± 1.37 Ma
5.78 ± 0.3 Ma
37-39°C
39-43°C
39-43°C
Cdy; 6.29 ± 0.30 Ma
37-45°C
43-45°C
45-57°C
45-57°C
Tuff
1 cm
B
ESF 13+19
MGSC
69-73°C
69-75°C
1.70 ± 0.02 Ma
57-67°C
59-65°C
67-75°C
Cdy;
4.00 ± 1.46 Ma
Tuff
1 cm
C
ESF 28+80
Liquid-only
0.38 ± 0.02 Ma (n = 2)
MGSC
Liquid-only
3.88 ± 0.11 Ma (n = 3)
35-41°C
35-41°C
Tuff
39-41°C
35-45°C
49-55°C
39-45°C
Tuff
1 cm
D
ESF 72+25
MGSC
Bladed calcite
2.90 ± 0.06 Ma
Tuff
1 cm
E
ESF 04+73.4
Liquid-only inclusions
MGSC
69-79°C
71-81°C
73-79°C
71-83°C
75-81°C
2-phase FIAs
9.06 ± 0.08 Ma
Cdy - Qtz - Brown opal
1 cm
F

Figure 7

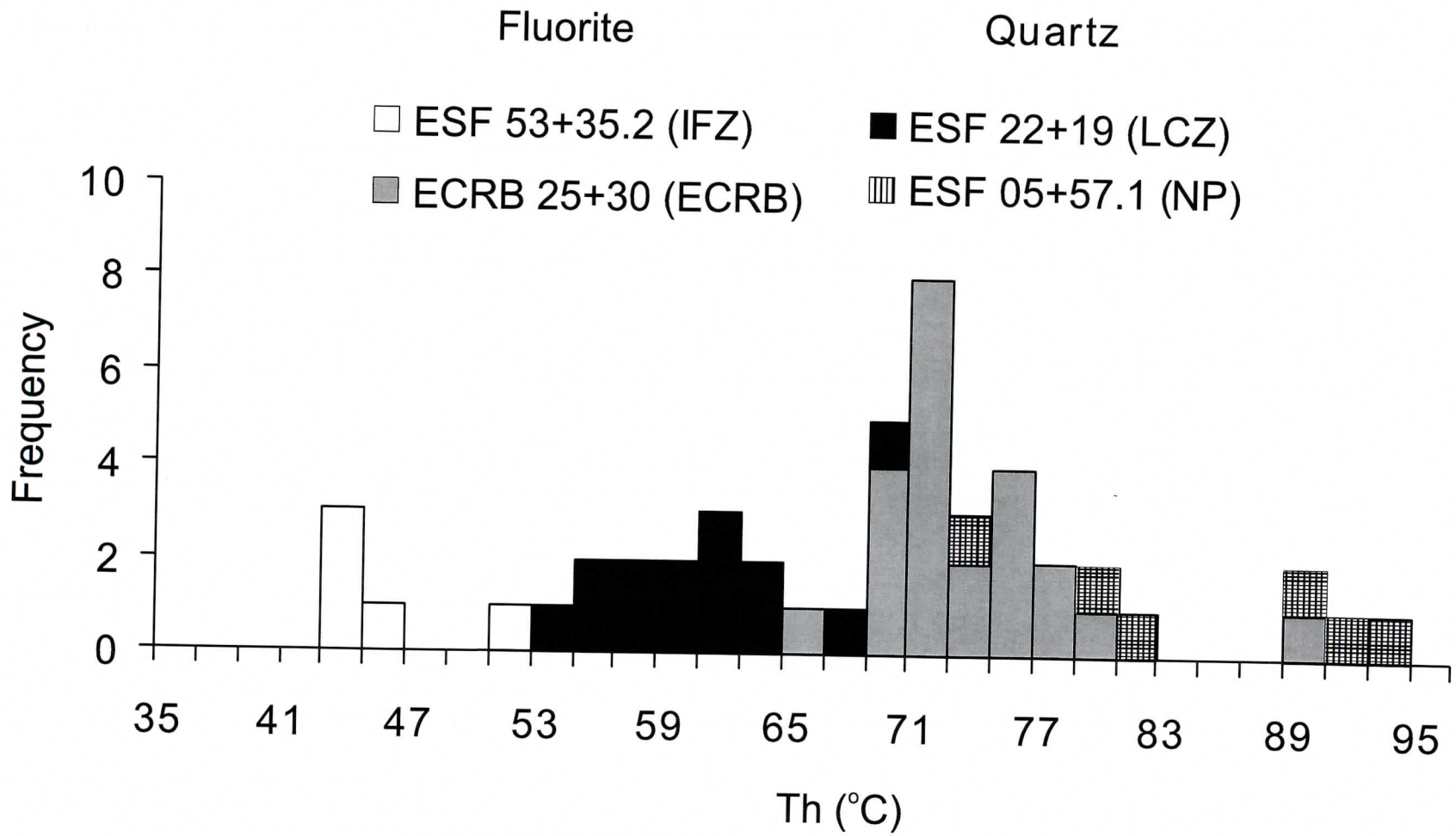
Fluorite
Quartz
ESF 53+35.2 (IFZ)
ECRB 25+30 (ECRB)
ESF 22+19 (LCZ)
ESF 05+57.1 (NP)
Frequency
10
8
6
4
2
0
35
41
47
53
59
65
71
77
83
89
95
Th (°C)

Figure 8

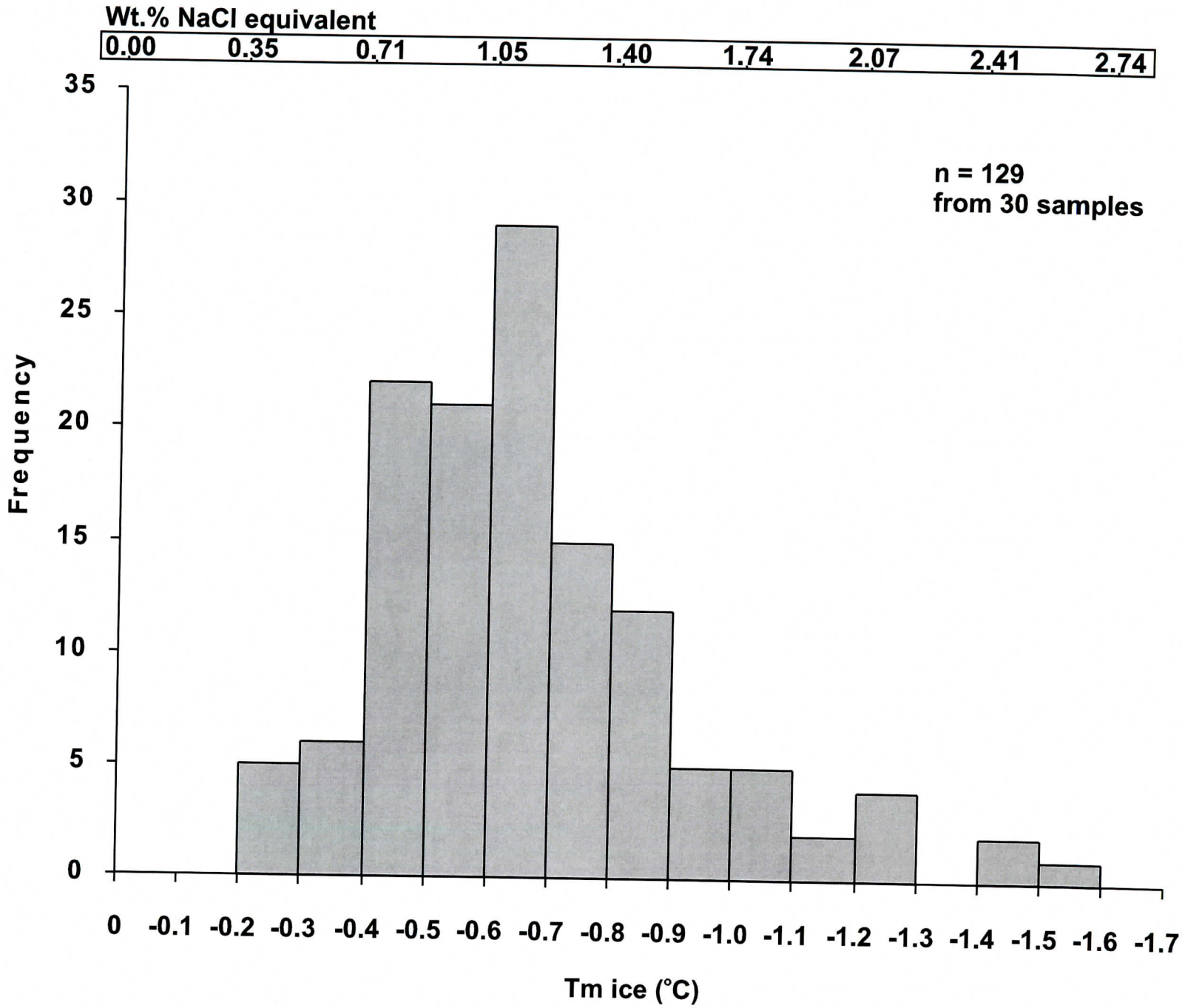
Wt.% NaCl equivalent
0.00
0.35
0.71
1.05
1.40
1.74
2.07
2.41
2.74
n = 129
from 30 samples
Frequency
35
30
25
20
15
10
5
0
0
-0.1
-0.2
-0.3
-0.4
-0.5
-0.6
-0.7
-0.8
-0.9
-1.0
-1.1
-1.2
-1.3
-1.4
-1.5
-1.6
-1.7
Tm ice (°C)

Figure 9

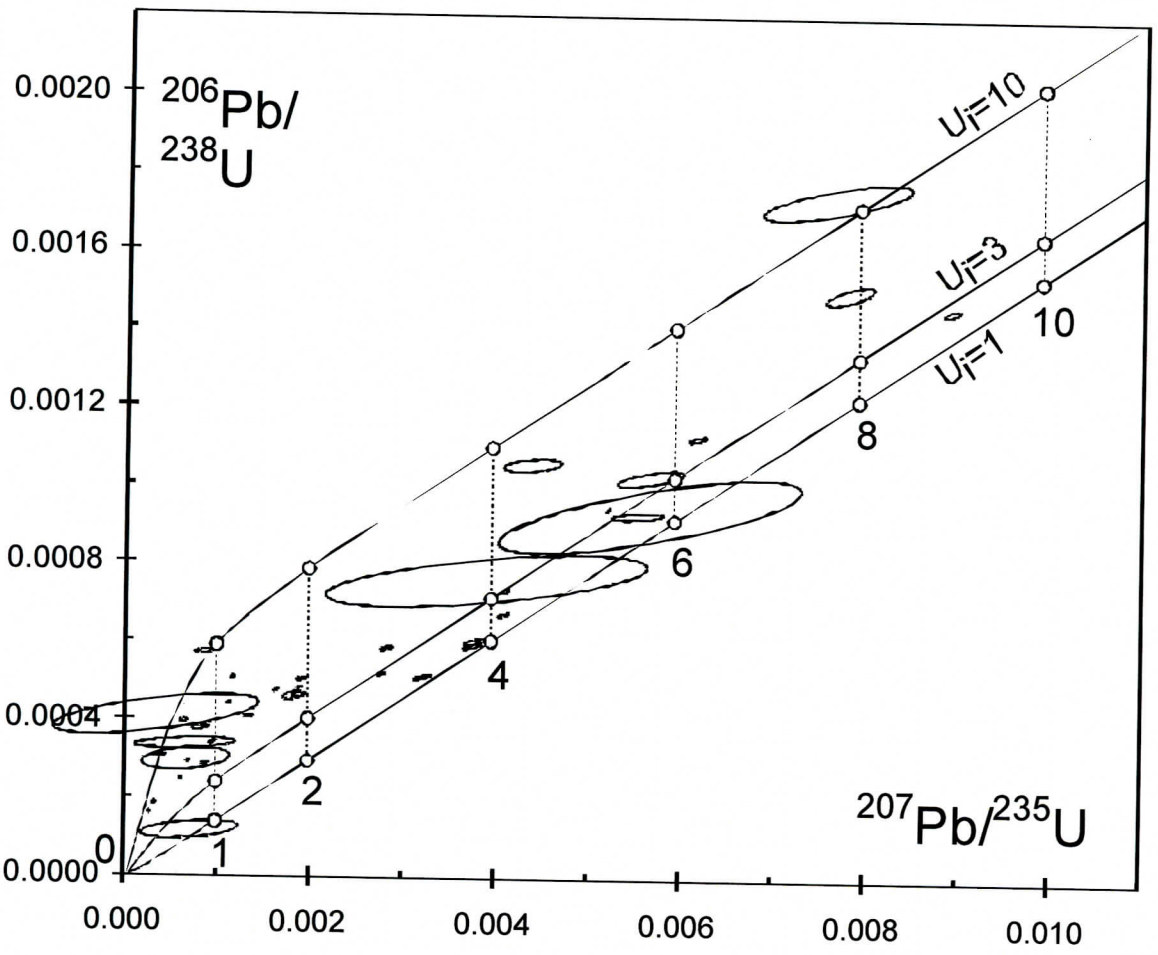
0.0020
0.0016
0.0012
0.0008
0.0004
0.0000
206Pb/
238U
Ui=10
Ui=3
Ui=1
0
1
2
4
6
8
10
0.000
0.002
0.004
0.006
0.008
0.010
207Pb/235U

Figure 10

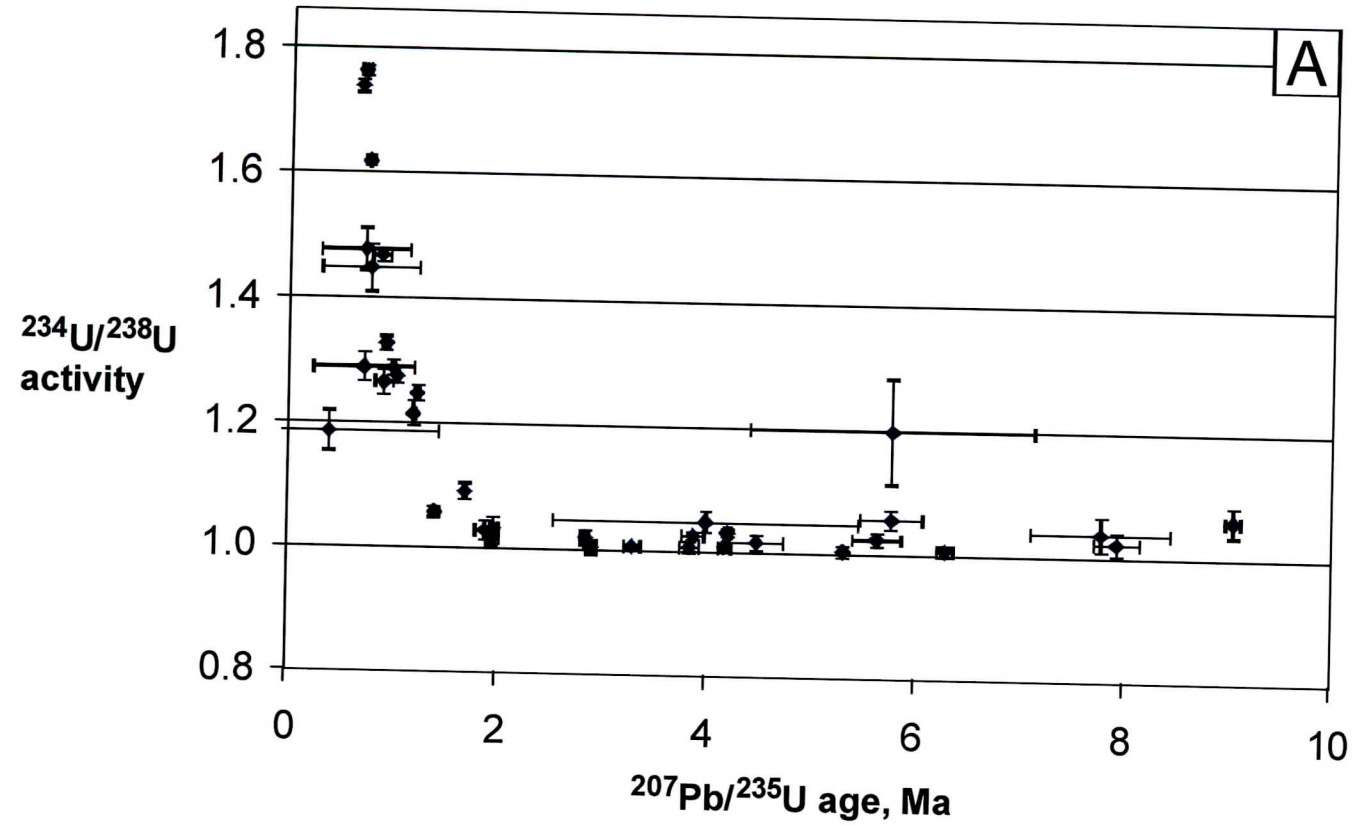
A
1.8
1.6
1.4
1.2
1.0
0.8
0
2
4
6
8
10
234U/238U activity
207Pb/235U age, Ma

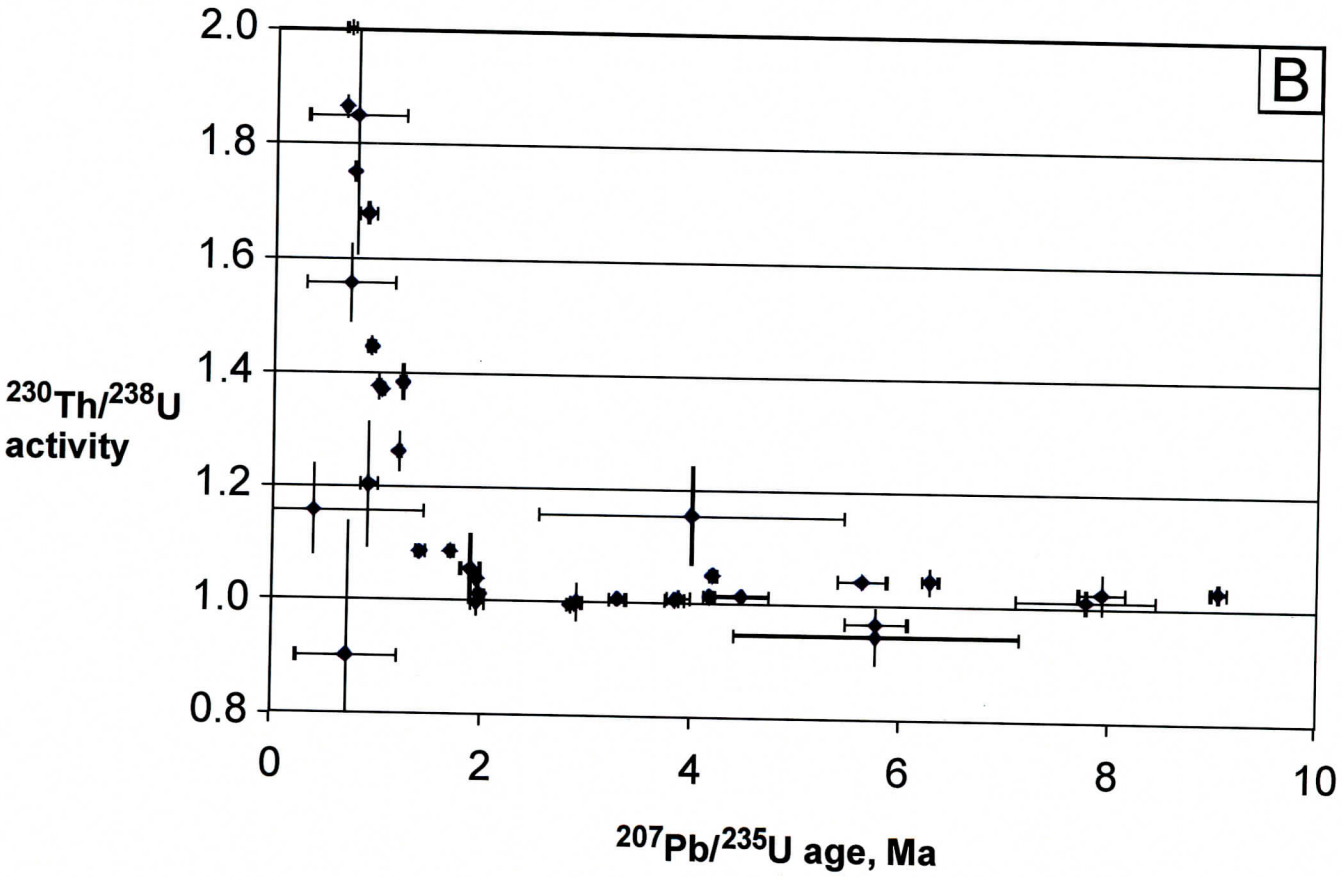
B
2.0
1.8
1.6
1.4
1.2
1.0
0.8
0
2
4
6
8
10
230Th/238U activity
207Pb/235U age, Ma

Figure11

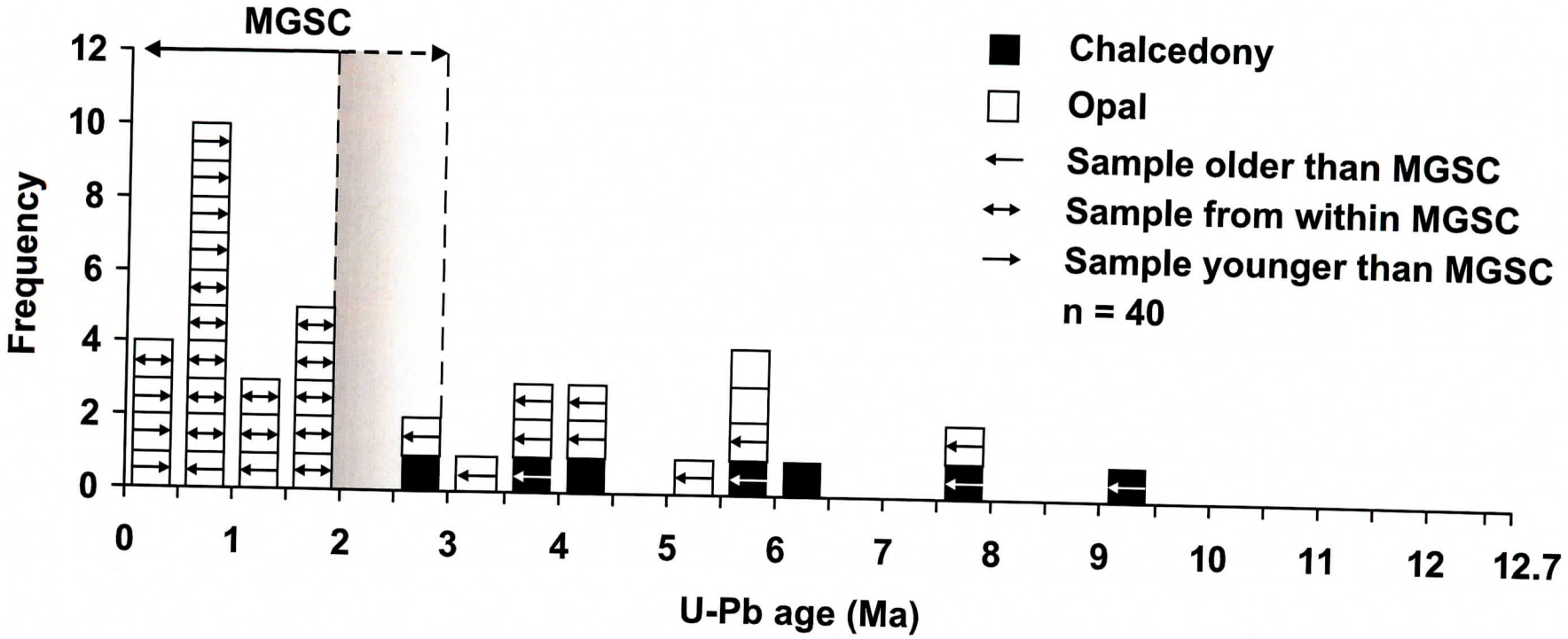
MGSC
Frequency
12
10
8
6
4
2
0
0
1
2
3
4
5
6
7
8
9
10
11
12
12.7
U-Pb age (Ma)
Chalcedony
Opal
Sample older than MGSC
Sample from within MGSC
Sample younger than MGSC
n = 40

Figure 12

Table 1. δD compositions of fluid inclusion fluids

Sample Number	δD (‰)	Mean δD (‰)	Description	Th (°C)
AL#5 00+28.5	-120, -90	-105	Outer part of mineral crust - Intermediate calcite	35 - 45
ESF 27+84	-110, -115*	-112.5	MGSC	< 35
ESF 60+52.5	-131*	-131	MGSC	< 35

* Duplicate analyses were performed by the conventional technique of heating the sample in a vacuum with an external furnace. H_2O is collected in a 6 mm diameter Pyrex tube with "magic" Indiana zinc. The tube is sealed off, heated to 550°C and the Zn reacts with H_2O to make ZnO + H_2. The H_2 is cracked directly into the mass spectrometer and analyzed using the dual inlet-bellows system.

Table 2. U-Th-Pb isotopic data.

No	Sample, fraction	Fraction weight (mg)	ppm U	ppb Th	Th/U	pg Com Pb (a)	$^{206}Pb/^{204}Pb$ (b)	2σ% err	$^{206}Pb/^{204}Pb$ (c)	2σ% err	$^{207}Pb/^{204}Pb$ (c)	$^{208}Pb/^{204}Pb$ (c)	$^{238}U/^{204}Pb$ (c)	$^{234}U/^{238}U_{act.}$ (d)	2σ% err	$^{230}Th/^{238}U_{act.}$ (d)	2σ% err
1	AL#5 00+28.5 Cdy-1(1)	1.505	28.5	0.64	2.2E-05	15.8	215.7	0.15	218.9	0.40	23.58	39.29	177,877	1.0062	0.82	1.0453	2.38
2	AL#5 00+28.5 Op-1a(1)	0.111	32.7	b.d.l.	n.d.	4.91	69.1	0.31	73.0	1.75	17.79	38.09	52,948	1.0557	1.52	0.9692	2.79
3	AL#5 00+28.5 Op-2a(1)	0.030	49.4	b.d.l.	n.d.	9.70	28.8	0.22	28.4	0.45	16.04	37.81	10,346	1.1983	7.11	0.9471	5.24
4	ECRB 01+25 Op-1(1)	0.028	26.5	48.49	1.8E-03	0.40	55.9	2.20	78.6	64.3	18.27	36.10	514,770	1.4480	2.64	1.8498	13.23
5	ECRB 07+40.5 Op-1(1)	0.124	156	54.55	3.5E-04	0.64	693.8	0.98	1283	17.90	41.44	37.37	3,685,500	1.2745	0.95	1.3711	0.90
6	ECRB 07+40.5 Op-2(1)	0.336	77.5	2.24	2.9E-05	0.92	472.2	0.79	683.6	9.65	27.55	38.33	2,702,410	1.7386	0.58	1.8656	1.14
7	ECRB 14+49 Op-1(1)	0.041	316	119.6	3.8E-04	0.33	1303	2.00	15375	223	270.18	54.12	30,299,600	1.2476	1.02	1.3833	2.39
8	ESF 04+44 Op-1(1)	0.518	373	64.50	1.7E-04	25.3	375.9	0.18	380.8	0.31	30.37	38.76	495,379	1.0305	0.55	1.0505	0.92
9	ESF 04+73.4 Op-1(1)	2.685	21.5	2.28	1.1E-04	13.4	419.5	0.53	428.5	0.71	33.82	38.35	281,460	1.0594	2.23	1.0313	1.55
10	ESF 05+09.1 Op-1(1)	0.150	39.5	10.09	2.6E-04	1.27	196.0	0.98	243.1	5.95	18.04	39.81	393,176	1.2649	1.56	1.2045	9.20
11	ESF 05+57.1 Cdy-1(1)	0.470	n.d.	n.d.	n.d.	n.d.	n.d.	n.d.	n.d.	n.d.	n.d.	n.d.	n.d.	1.0237	0.95	1.0374	7.86
12	ESF 05+57.1 Cdy-1(2)	0.062	160	b.d.l.	n.d.	1.48	247.5	0.43	358.6	9.92	28.73	38.89	654,552	1.0194	1.14	0.9956	1.67
13	ESF 05+57.1 Cdy-2(1)	0.799	42.2	9.95	2.4E-04	10.9	227.3	2.10	232.9	2.23	22.08	32.89	203,314	1.0162	1.22	1.0144	1.44
14	ESF 13+19 Cdy-2(1)	0.672	74.4	4.81	6.5E-05	216	30.1	0.74	30.1	0.75	16.04	37.42	14,898	1.0475	1.62	1.1555	7.60
15	ESF 13+19 Op-1(1)	0.418	123	3.05	2.5E-05	4.00	412.8	0.36	444.0	1.63	26.15	39.99	894,429	1.0899	1.23	1.0870	0.81
16	ESF 27+84 Op-1(1)	0.148	160	0.53	3.3E-06	0.63	1179	1.80	2232	18.6	78.13	38.41	4,590,870	1.0234	0.81	1.0392	1.80
17	ESF 27+84 Op-1(2)	0.046	130	8.21	6.3E-05	0.95	214.0	1.40	2240	218	78.89	34.24	4,818,200	1.0276	1.47	1.0559	5.86
18	ESF 27+84 Op-1(3)	0.066	153	2.89	1.9E-05	2.34	150.0	0.57	222.1	10.9	21.60	37.70	439,300	1.0141	0.96	0.9974	2.41
19	ESF 27+84 Op-2(1)	0.175	103	2.65	2.6E-05	0.68	525.7	0.84	1411	35.7	39.44	35.20	4,783,750	1.6189	0.45	1.7522	1.04
20	ESF 27+84 Op-2(2)	0.280	88.6	0.56	6.3E-06	1.17	481.8	0.89	1788	57.0	51.05	42.12	5,248,790	1.2877	1.02	1.3759	1.73
21	ESF 27+84 Op-3(1)	0.161	276	238.1	8.6E-04	0.72	3748	1.10	6503	14.8	275.52	37.78	6,883,780	1.0036	0.95	n.d.	n.d.
22	ESF 27+84 Op-3a(1)	0.049	192	b.d.l.	n.d.	0.88	372.5	0.91	830.5	26.6	37.79	38.75	1,611,180	1.0309	1.75	1.0111	2.14
23	ESF 27+84 Op-4a(1)	0.007	122	b.d.l.	n.d.	1.01	44.0	0.80	51.1	13.7	16.14	37.02	109,001	1.4777	2.29	1.5562	4.41
24	ESF 27+84 Op-5a(1)	0.114	129	34.85	2.7E-04	1.30	322.0	1.20	506.1	12.5	27.20	38.18	1,194,820	1.0566	0.81	1.0860	1.04
25	ESF 27+84 Op-6a(1)	0.022	79.5	198.1	2.5E-03	6.36	27.4	0.47	26.7	0.74	15.67	38.18	19,160	1.1853	2.76	1.1580	7.01
26	ESF 28+80 Op-1(1)	0.316	127	b.d.l.		14.7	108.6	0.25	110.1	0.44	19.77	38.94	178,630	1.0057	0.45	1.0075	0.46
27	ESF 28+80 Op-1(2)	0.274	98.9	0.54	5.5E-06	12.6	102.6	0.33	108.3	1.29	19.69	38.92	148,603	1.0243	0.59	1.0089	1.43
28	ESF 28+80 Op-1(3)	0.356	127	0.46	3.6E-06	18.8	109.9	0.23	114.1	0.85	20.01	39.16	161,374	1.0072	0.85	1.0070	1.42
29	ESF 28+80 Op-2(1)	0.453	82.1	2.05	2.5E-05	1.67	251.8	0.66	494.5	20.9	21.45	38.03	2,968,300	3.6667	0.32	3.5906	0.60
30	ESF 28+80 Op-2(2)	0.245	90.0	1.91	2.1E-05	1.32	221.8	0.75	598.0	37.8	23.04	39.13	3,154,360	3.3338	0.57	3.4200	1.50
31	ESF 29+11 Op-1(1)	0.156	44.1	5.99	1.4E-04	0.83	190.1	1.40	272.1	10.9	17.82	40.69	831,669	3.4335	1.42	3.5109	2.00
32	ESF 29+11 Op-2(1)	0.167	177	21.33	1.2E-04	1.93	456.9	0.31	535.1	3.64	25.18	39.46	1,170,930	1.2144	1.63	1.2620	2.89
33	ESF 32+31 Cdy-1(1)	0.861	17.3	1.32	7.6E-05	15.0	114.3	0.16	115.9	0.39	19.29	39.52	64,892	1.0213	1.77	1.0257	3.54
34	ESF 60+52.5 Op-1(1)	0.071	71.4	b.d.l.	n.d.	1.34	116.4	0.64	136.5	5.11	17.47	37.96	311,924	1.4685	0.72	1.6793	1.23
35	ESF 60+52.5 Op-1(2)	0.105	61.3	0.27	4.4E-06	0.61	297.4	0.91	543.7	19.0	21.76	38.27	1,329,590	1.7628	0.45	2.0037	0.68
36	ESF 64+95 Op-1(1)	0.959	90.1	1.90	2.1E-05	23.5	177.6	0.14	184.3	0.83	22.91	39.61	246,611	1.0076	0.47	1.0136	1.13
37	ESF 67+81 Op-1(1)	0.611	62.9	2.96	4.7E-05	6.94	348.0	3.30	362.6	3.56	30.49	37.52	371,335	1.0235	1.11	1.0436	1.15
38	ESF 72+25 Op-1(1)	0.078	131	10.78	8.2E-05	1.91	222.7	0.60	256.4	3.58	23.92	37.16	407,065	1.0034	1.16	1.0010	3.38
39	ESF 76+59.5 Op-1(1)	0.578	8.1	21.75	2.7E-03	14.2	55.9	0.28	56.15	0.42	16.81	39.65	21,514	1.0370	2.76	1.0126	2.05
40	ESF 76+59.5 Op-2(1)	0.024	63.3	52.68	8.3E-04	0.57	91.5	3.30	139.8	20.9	17.33	36.07	359,910	1.2885	1.77	0.9026	26.15
41	ESF 76+59.5 Op-2(2)	0.118	68.3	8.54	1.3E-04	0.50	331.3	1.10	776.4	30.6	32.23	39.16	2,649,140	1.3271	0.85	1.4458	1.13

n.d. - not determined

b.d.l.-below detection limit (amount of Th in an analysis is indistinguishable from analytical blank)

Sample names: Op-opal, Cdy-Chalcedony. Numbers in parentheses indicate replicate analyses.

a) Total common Pb content in analysis, including initial common Pb and procedure blank.

b) Measured ratios, corrected for fractionation only.

c) Isotopic ratios, corrected for fractionation, spike contribution, and procedure blank.

d) Activity ratios, calculated from measured isotopic ratios corrected for fractionation, spike contribution, and procedure blank.

Table 3. U-Th-Pb isotopic ratios and U-Pb ages.

No	Sample, fraction	$^{206}Pb^*/^{238}U$	2σ% err	$^{207}Pb^*/^{235}U$	2σ% err	Rho	$^{207}Pb^*/^{206}Pb^*$	2σ% err	$^{206}Pb^*/^{238}U$ Age (Ma)	2σ err	$^{207}Pb^*/^{235}U$ Age (Ma)	$^{207}Pb^*/^{235}U$ Age (Ma)	2σ err	$^{207}Pb^*/^{206}Pb^*$ Age (Ma)	$^{234}U/^{238}U_{act.}$ initial
		(a)		(a)		(b)	(a)		(c)		(c)	(d)		(c)	(e)
1	AL#5 00+28.5 Cdy-1(1)	0.0011246	0.51	0.006167	1.27	0.725	0.0398	0.96	7.245	0.037	6.243	6.290	0.080	-366	4.02
2	AL#5 00+28.5 Op-1a(1)	0.0010223	1.64	0.005660	5.22	0.669	0.0402	4.30	6.587	0.108	5.731	5.777	0.302	-341	3.61
3	AL#5 00+28.5 Op-2a(1)	0.0009257	8.52	0.005661	23.70	0.737	0.0444	18.30	5.965	0.508	5.731	5.778	1.369	-91	1.84
4	ECRB 01+25 Op-1(1)	0.0001161	16.00	0.000710	60.40	0.429	0.0444	55.40	0.748	0.120	0.721	0.768	0.464	-90	1.31
5	ECRB 07+40.5 Op-1(1)	0.0003431	0.44	0.000966	1.42	0.387	0.0204	1.32	2.211	0.010	0.980	1.028	0.015	-2546	4.98
6	ECRB 07+40.5 Op-2(1)	0.0002460	0.41	0.000609	2.12	0.325	0.0179	2.02	1.586	0.006	0.618	0.665	0.014	-3144	4.75
7	ECRB 14+49 Op-1(1)	0.0005068	0.47	0.001158	1.71	0.335	0.0166	1.62	3.266	0.015	1.176	1.223	0.021	-3560	7.40
8	ESF 04+44 Op-1(1)	0.0007306	0.43	0.004106	0.76	0.760	0.0408	0.51	4.708	0.020	4.161	4.208	0.032	-303	2.73
9	ESF 04+73.4 Op-1(1)	0.0014554	0.47	0.008914	0.84	0.685	0.0444	0.62	9.375	0.044	9.011	9.057	0.076	-87	2.21
10	ESF 05+09.1 Op-1(1)	0.0005704	0.67	0.000848	9.58	0.361	0.0108	9.35	3.676	0.025	0.861	0.907	0.087	<<0	10.19
11	ESF 05+57.1 Cdy-1(1)														
12	ESF 05+57.1 Cdy-1(2)	0.0005191	0.66	0.002761	1.38	0.604	0.0386	1.11	3.346	0.022	2.799	2.847	0.039	-446	2.73
13	ESF 05+57.1 Cdy-2(1)	0.0010531	1.23	0.004380	5.89	0.379	0.0302	5.54	6.785	0.083	4.437	4.485	0.264	-1142	7.84
14	ESF 13+19 Cdy-2(1)	0.0007571	7.36	0.003899	36.50	0.589	0.0374	32.70	4.879	0.359	3.951	3.999	1.460	-531	3.81
15	ESF 13+19 Op-1(1)	0.0004753	0.63	0.001623	1.25	0.637	0.0248	0.98	3.063	0.019	1.647	1.695	0.021	-1792	5.25
16	ESF 27+84 Op-1(1)	0.0004821	0.28	0.001878	0.97	0.390	0.0282	0.90	3.107	0.009	1.905	1.952	0.019	-1348	4.61
17	ESF 27+84 Op-1(2)	0.0004610	1.86	0.001811	4.95	0.450	0.0285	4.43	2.971	0.055	1.837	1.885	0.093	-1321	4.42
18	ESF 27+84 Op-1(3)	0.0004628	1.10	0.001878	3.32	0.485	0.0294	2.95	2.983	0.033	1.905	1.953	0.065	-1219	4.25
19	ESF 27+84 Op-2(1)	0.0002910	0.54	0.000687	2.07	0.332	0.0171	1.96	1.876	0.010	0.697	0.744	0.015	-3388	5.28
20	ESF 27+84 Op-2(2)	0.0003371	0.73	0.000931	2.15	0.391	0.0200	1.98	2.173	0.016	0.945	0.991	0.021	-2630	5.02
21	ESF 27+84 Op-3(1)	0.0009420	0.32	0.005206	0.36	0.907	0.0401	0.15	6.070	0.019	5.272	5.319	0.019	-346	3.44
22	ESF 27+84 Op-3a(1)	0.0005038	0.67	0.001897	2.25	0.372	0.0273	2.10	3.247	0.022	1.924	1.972	0.044	-1457	4.95
23	ESF 27+84 Op-4a(1)	0.0002962	7.89	0.000662	58.40	0.307	0.0162	56.50	1.909	0.151	0.672	0.718	0.420	-3690	5.55
24	ESF 27+84 Op-5a(1)	0.0004078	0.71	0.001336	3.12	0.355	0.0238	2.95	2.629	0.019	1.356	1.404	0.044	-1942	4.89
25	ESF 27+84 Op-6a(1)	0.0004090	10.50	0.000337	269.00	0.642	0.0060	262.00	2.636	0.277	0.342	0.389	1.047	<<0	13.59
26	ESF 28+80 Op-1(1)	0.0005107	0.92	0.003202	2.43	0.738	0.0455	1.86	3.291	0.030	3.246	3.294	0.080	-30	1.31
27	ESF 28+80 Op-1(2)	0.0006018	0.99	0.003779	2.77	0.680	0.0455	2.22	3.878	0.039	3.830	3.877	0.107	-27	1.32
28	ESF 28+80 Op-1(3)	0.0005903	0.91	0.003747	2.32	0.732	0.0460	1.77	3.804	0.035	3.798	3.845	0.089	<<0	1.20
29	ESF 28+80 Op-2(1)	0.0001602	0.89	0.000271	4.67	0.299	0.0123	4.49	1.033	0.009	0.275	0.322	0.015	<<0	6.27
30	ESF 28+80 Op-2(2)	0.0001836	1.26	0.000324	5.82	0.297	0.0128	5.57	1.183	0.015	0.329	0.376	0.022	<<0	6.05
31	ESF 29+11 Op-1(1)	0.0003046	0.99	0.000366	17.90	0.258	0.0087	17.60	1.963	0.019	0.371	0.418	0.075	<<0	9.30
32	ESF 29+11 Op-2(1)	0.0004409	0.60	0.001125	1.35	0.574	0.0185	1.12	2.842	0.017	1.142	1.190	0.016	-2991	6.26
33	ESF 32+31 Cdy-1(1)	0.0014964	1.26	0.007803	2.78	0.730	0.0378	2.05	9.639	0.121	7.892	7.938	0.221	-498	6.14
34	ESF 60+52.5 Op-1(1)	0.0003772	1.10	0.000816	9.34	0.430	0.0157	8.92	2.431	0.027	0.828	0.875	0.082	-3879	6.38
35	ESF 60+52.5 Op-1(2)	0.0003948	0.73	0.000636	5.85	0.242	0.0117	5.72	2.544	0.019	0.646	0.693	0.041	<<0	7.99
36	ESF 64+95 Op-1(1)	0.0006711	0.56	0.004078	1.33	0.756	0.0441	0.98	4.324	0.024	4.132	4.180	0.056	-107	1.72
37	ESF 67+81 Op-1(1)	0.0009258	0.80	0.005523	4.17	0.404	0.0433	3.92	5.965	0.048	5.593	5.639	0.235	-152	2.24
38	ESF 72+25 Op-1(1)	0.0005836	0.68	0.002813	1.90	0.558	0.0350	1.62	3.761	0.026	2.852	2.900	0.055	-712	3.76
39	ESF 76+59.5 Op-1(1)	0.0017348	2.21	0.007652	8.61	0.728	0.0320	7.16	11.174	0.247	7.741	7.787	0.670	-966	10.92
40	ESF 76+59.5 Op-2(1)	0.0003362	3.36	0.000655	67.70	0.365	0.0141	66.50	2.167	0.073	0.665	0.712	0.482	<<0	6.50
41	ESF 76+59.5 Op-2(2)	0.0002860	0.84	0.000864	3.60	0.315	0.0219	3.43	1.843	0.016	0.877	0.924	0.033	-2252	4.27

a) Pb/U ratios, corrected for fractionation, spike, blank, and initial common Pb.
b) Error correlation between $^{207}Pb^*/^{235}U$ and $^{206}Pb^*/^{238}U$.
c) Conventional ages calculated assuming initial radioactive secular equilibrium.
d) Disequilibrium $^{207}Pb^*/^{235}U$ age calculated assuming zero initial activity of ^{231}Pa and ^{227}Ac. Ages used in this study.
e) Initial activity ratio calculated from $^{207}Pb^*/^{235}U$ disequilibrium age and measured $^{206}Pb^*/^{238}U$ assuming closed system behavior.

APPENDIX – ADDITIONAL DESCRIPTIONS OF DATED SAMPLES

In all samples the locations of 2–phase FIAs are marked by black squares and those that were used for microthermometry are marked with yellow squares. Homogenization temperatures are adjacent to the 2–phase FIA locations. The locations of material sampled for dating are shown in red and dated material was opal unless specified as chalcedony. A dashed black line shows the contact between MGSC and earlier minerals.

ECRB 01+25 – Lithophysal cavity sample with bladed calcite overgrown by MGSC and associated brown opal. No 2–phase FIAs were observed in this sample. Calcite dissolution is indicated by the presence of irregular calcite blades, abundant porosity, and the presence of brown opal from the base of the sample to the outermost surface (with MGSC). Textures indicate that brown opal is associated with precipitation of MGSC. Brown opal filling a pore in the basal part of the crust has a U-Pb age of 0.77 ± 0.46 Ma. This sample indicates that brown opal can be relatively young.

ECRB 07+40.5 – Lithophysal cavity sample with older moderately fine-grained, darker calcite and bladed calcite overgrown by MGSC. Two–phase FIAs were not observed in this sample. Two opal samples were dated, one from within the MGSC and one from the outermost surface that is partially overgrown by younger MGSC. Opal from within the MGSC gave an age of 1.03 ± 0.01 Ma and opal from the outermost part of the crust gave an U-Pb age of 0.67 ± 0.01 Ma. These ages indicate that MGSC precipitated before and after 1.03 ± 0.01 Ma.

ECRB 14+49 – Lithophysal cavity sample with fine-grained calcite at the base overgrown by bladed calcite, which is in turn, overgrown by MGSC. No 2–phase FIAs were observed in this sample. An opal sample was collected along the boundary between bladed calcite and the MGSC and gave a U-Pb age of 1.22 ± 0.02 Ma, indicating that MGSC precipitated after this time.

ESF 04+44 – Fracture sample with layers of chalcedony overgrown by brown opal and MGSC. No 2–phase FIAs were identified in this sample. Brown layered opal has an age of 4.21 ± 0.03 Ma and MGSC precipitated after this time.

ESF 05+09.1 – Fracture sample containing chalcedony and quartz overgrown by MGSC and an outer layer of brown opal (red). No 2–phase FIAs are present in this sample. Brown opal from the outermost surface has an age of 0.91 ± 0.09 Ma and MGSC is older than this age. This sample also shows that brown opal can be young.

ESF 05+57.1 – Fracture with chalcedony-quartz and fluorite at the base of the crust overgrown by layers of chalcedony-brown opal with minor fluorite. Two-phase FIAs occur in basal quartz but not in outer minerals. Chalcedony in the outer part of the sample forms thin layers within opal layers and has an age of 4.49 ± 0.26 Ma indicating that the 2-phase FIAs in quartz are older than this age. Younger chalcedony precipitated in open space in the central region of the section and has an age of 2.85 + 0.04 Ma.

ESF 29+11 – Lithophysal cavity sample containing fine-grained dark calcite at base overgrown by bladed calcite, which was overgrown by intergrown MGSC and opal. Two–phase FIAs occur in the basal calcite and basal bladed calcite but not in outer bladed calcite or MGSC. Opal from within the MGSC layer has an age of 1.19 ± 0.02 Ma and MGSC precipitated before and after this time. Opal from the outer most surfaces that is partially overgrown by MGSC has an age of 0.42 ± 0.08 Ma, indicating that the MGSC precipitated before and after this time.

ESF 32+31 – Lithophysal cavity sample containing basal calcite containing chalcedony after calcite, overgrown by bladed calcite and an outer layer of MGSC. Two–phase FIAs occur in basal calcite but their temporal relationship to the chalcedony layer is ambiguous owing to lateral variations in the crust. The chalcedony had an age of 7.94 ± 0.22 Ma and bladed calcite and MGSC are younger than this age.

ESF 60+52.5 – Fracture sample containing minor early calcite overgrown by MGSC. An opal layer within the center of the MGSC has ages of 0.69 ± 0.04 and 0.88 ± 0.08 Ma and MGSC formed before and after this time. No 2–phase FIAs occur in this sample.

ESF 64+95 – Lithophysal cavity sample with basal calcite containing 2–phase FIAs overgrown by chalcedony-brown opal-quartz after early calcite, by bladed calcite, and then by MGSC. No 2–phase FIAs are present in the bladed calcite or MGSC. Brown opal associated with quartz has an age of 4.18 ± 0.06 Ma and bladed calcite and MGSC are younger than this age.

ESF 67+81 – Fracture sample containing basal calcite overgrown by chalcedony-brown opal-calcite-quartz, overgrown by MGSC. No 2–phase FIAs occur in this sample. Brown opal below the quartz layer and MGSC has an age of 5.64 ± 0.24 Ma and MGSC precipitated after this time.

ESF 76+59.5 – Fracture sample with brown opal adjacent to wall rock. Brown opal is overgrown by clear bladed calcite, which is overgrown by brown opal and then by MGSC. No 2–phase FIAs were identified in this sample. Brown opal from the base of the section gave an age of 7.79 ± 0.67 Ma. Opal on the boundary between bladed calcite and MGSC has an age between 0.71 ± 0.48 Ma and 0.92 ± 0.03 Ma indicating that MGSC precipitated after this time.

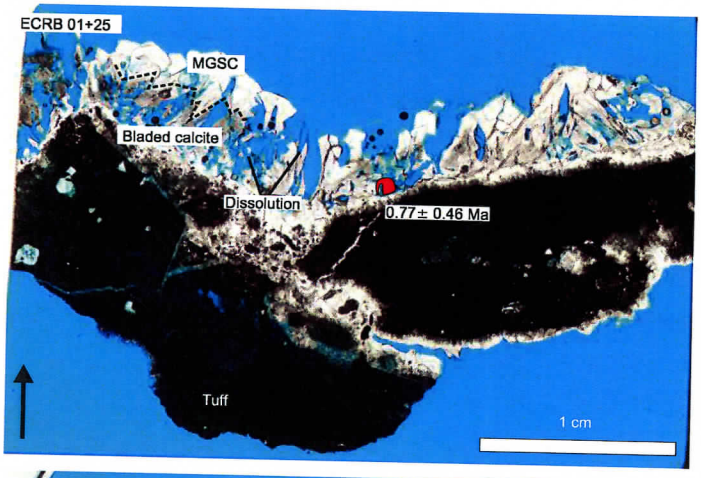
ECRB 01+25
MGSC
Bladed calcite
Dissolution
0.77± 0.46 Ma
Tuff
1 cm

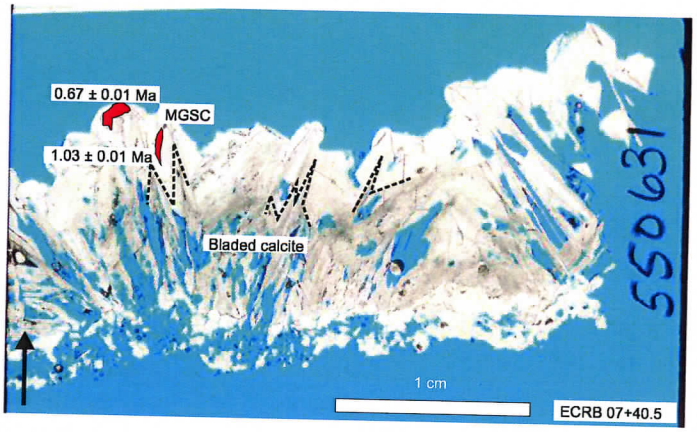
0.67 ± 0.01 Ma
MGSC
1.03 ± 0.01 Ma
Bladed calcite
1 cm
ECRB 07+40.5
550631

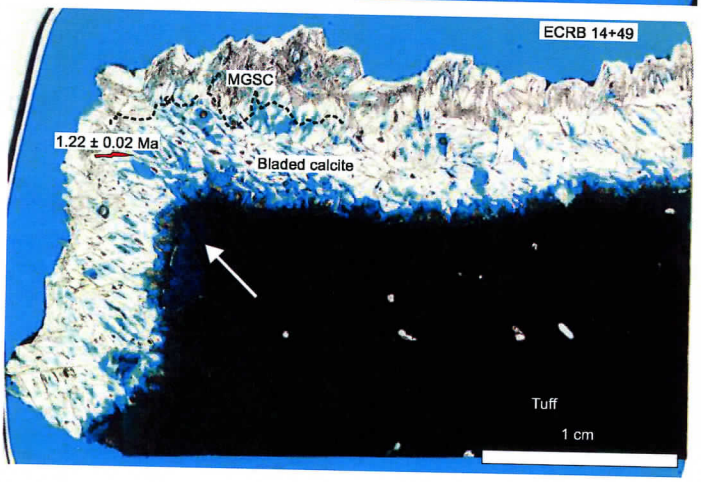
ECRB 14+49
MGSC
1.22 ± 0.02 Ma
Bladed calcite
Tuff
1 cm

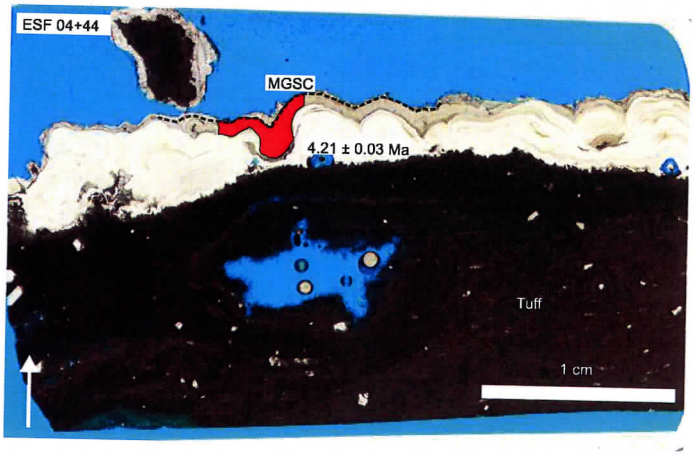
ESF 04+44
MGSC
4.21 ± 0.03 Ma
Tuff
1 cm

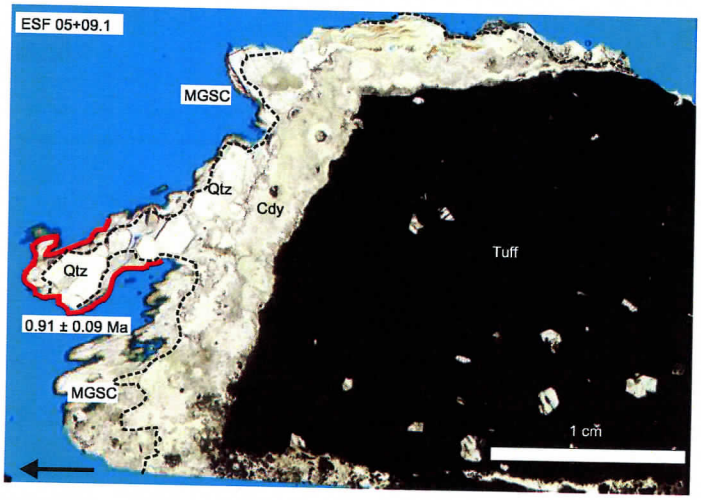
ESF 05+09.1
MGSC
Qtz
Cdy
Tuff
Qtz
0.91 ± 0.09 Ma
MGSC
1 cm

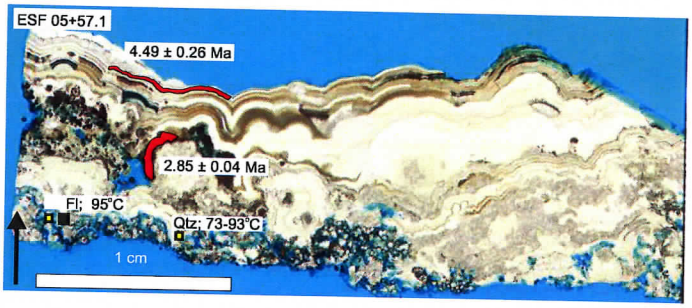
ESF 05+57.1
4.49 ± 0.26 Ma
2.85 ± 0.04 Ma
Fl; 95°C
Qtz; 73-93°C
1 cm

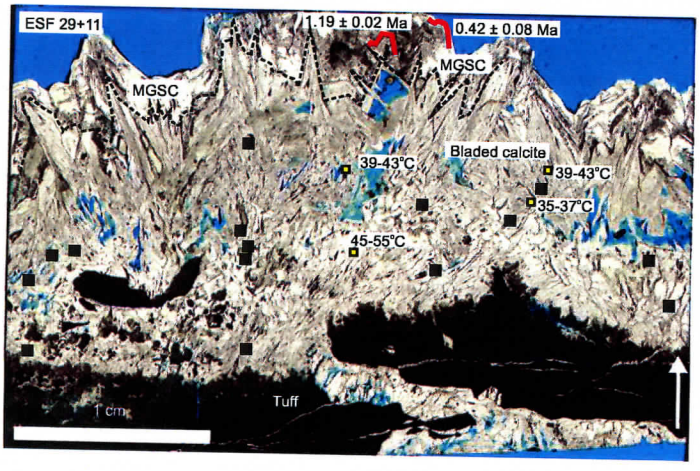
ESF 29+11
1.19 ± 0.02 Ma
0.42 ± 0.08 Ma
MGSC
MGSC
39-43°C
Bladed calcite
39-43°C
35-37°C
45-55°C
Tuff
1 cm

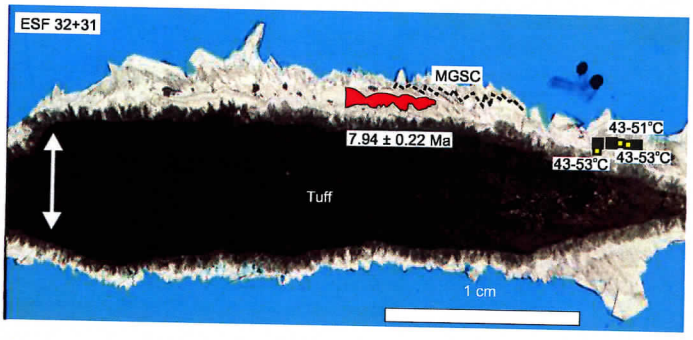
ESF 32+31
MGSC
7.94 ± 0.22 Ma
43-51°C
43-53°C
43-53°C
Tuff
1 cm

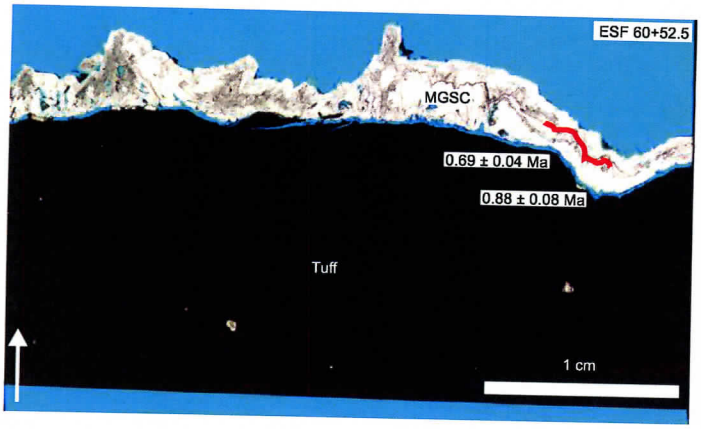
ESF 60+52.5
MGSC
0.69 ± 0.04 Ma
0.88 ± 0.08 Ma
Tuff
1 cm

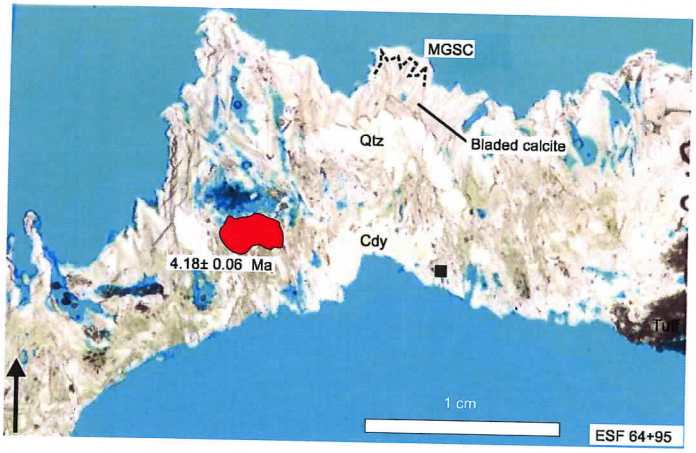
MGSC
Qtz
Bladed calcite
Cdy
4.18± 0.06 Ma
1 cm
ESF 64+95


ESF 67+81
MGSC
5.64 ± 0.24 Ma
Tuff
1 cm

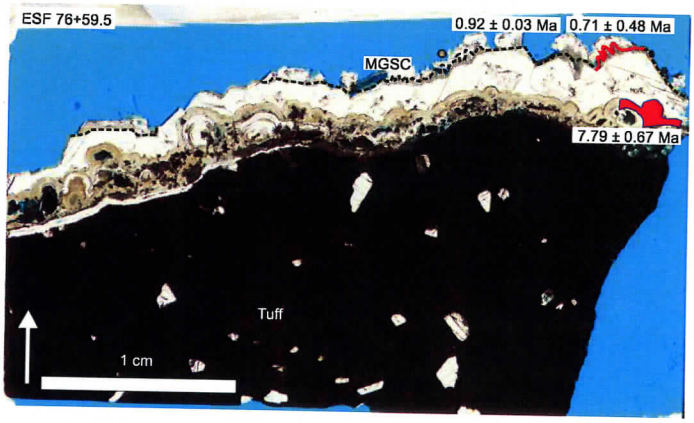
ESF 76+59.5
0.92 ± 0.03 Ma
0.71 ± 0.48 Ma
MGSC
7.79 ± 0.67 Ma
Tuff
1 cm